Available online at www.sciencedirect.com

ScienceDirect

Geochimica et Cosmochimica Acta 150 (2015) 171–191

Geochimica et Cosmochimica Acta

www.elsevier.com/locate/gca

Experimental evidence for kinetic effects on B/Ca in synthetic calcite: Implications for potential $B(OH)_4^-$ and $B(OH)_3$ incorporation

Joji Uchikawa [a,*], Donald E. Penman [b], James C. Zachos [b], Richard E. Zeebe [a]

[a] Department of Oceanography, SOEST, University of Hawaii at Manoa, 1000 Pope Road, Honolulu, HI 96822, United States
[b] Department of Earth and Planetary Sciences, University of California Santa Cruz, 1156 High Street, Santa Cruz, CA 95060, United States

Received 25 July 2014; accepted in revised form 26 November 2014; Available online 5 December 2014

Abstract

The boron to calcium ratio (B/Ca) in biogenic $CaCO_3$ is being increasingly utilized as a proxy for past ocean carbonate chemistry. However, B/Ca of cultured and core-top foraminifers show dependence on multiple physicochemical seawater properties and only a few of those have been inorganically tested for their impacts. Accordingly, our understanding of the controls on foraminiferal B/Ca and thus how to interpret B/Ca in fossil shells is incomplete. To gain a clearer understanding of the B incorporation mechanism, we performed inorganic calcite precipitation experiments using a pH-stat system. As previously reported, we confirm that B/Ca in calcite increases with both fluid pH and total B concentration (denoted as $[B_T]$, where $[B_T] = [B(OH)_3] + [B(OH)_4^-]$). We provide the first evidence that B/Ca also increases with the concentration of total dissolved inorganic carbon (DIC) and calcium ion. With the exception of the $[B_T]$ experiments, these chemical manipulations were accompanied by an increase in calcite saturation, and accordingly precipitation rate (denoted as R). But when pH and $[Ca^{2+}]$ were jointly varied at a fixed saturation level to maintain relatively constant R at different pH and $[Ca^{2+}]$ combinations, B/Ca was insensitive to both pH and $[Ca^{2+}]$ changes. These experimental results unequivocally suggest kinetic effects related to R on B/Ca. Furthermore, with a suite of chemical manipulations we found that the B/Ca variability is explicable by just R and the $[B_T]/[DIC]$ ratio in the parent fluids. This observation was particularly robust for relatively rapidly precipitated samples, whereas for relatively slowly precipitated samples, it was somewhat ambiguous whether the $[B_T]/[DIC]$ or $[B(OH)_4^-]/[HCO_3^-]$ ratio provides a better fit to the experimental data. Nonetheless, our experimental results can be considered as indirect evidence for incorporation of both $B(OH)_4^-$ and $B(OH)_3$ into calcite. We propose a simple mathematical expression to describe the mode of B incorporation into synthetic calcite that depends only on the fluid $[B_T]/[DIC]$ ratio and the precipitation rate R. This novel finding has important implications for future calibrations and applications of the B/Ca proxy as well as the $\delta^{11}B$ paleo-pH proxy.

1. INTRODUCTION

The change in the Earth's surface temperature per doubling of the atmospheric CO_2 concentration is referred to as climate sensitivity, which depends on the background climate state and an intricate balance of numerous feedback mechanisms operating on various timescales (Rohling et al., 2012; Zeebe, 2013). Climate sensitivity derived from continuous paleotemperature and paleo-CO_2 reconstruction is of crucial importance to reliably predict future climate change from anthropogenic CO_2 emissions. Ancient atmosphere trapped in Antarctic ice-cores provides direct CO_2 records

* Corresponding author.
E-mail address: uchikawa@hawaii.edu (J. Uchikawa).

http://dx.doi.org/10.1016/j.gca.2014.11.022
0016-7037/

only up to the last ~800 Kyr (Lüthi et al., 2008). One way to unravel CO_2 variations further back in time is to constrain ocean carbonate chemistry using pH estimates derived from stable boron isotopes ($\delta^{11}B$) of planktonic foraminiferal shells archived in marine sediments (Spivack et al., 1993; Sanyal et al., 1995, 1996; Pearson and Palmer, 2000; Hönisch and Hemming, 2005; Foster, 2008; Hönisch et al., 2009; Bartoli et al., 2011; Sanyal et al., 1997). Another potentially useful proxy to constrain ocean carbonate chemistry is the boron to calcium ratio (B/Ca) in foraminiferal shells. Relative to $\delta^{11}B$ measurements, B/Ca measurements are typically less demanding in terms of sample size requirement and analytical time (Hönisch et al., 2007; Rae et al., 2011; Yu et al., 2013; Penman et al., 2014). In addition, B/Ca analysis using inductively coupled plasma-mass spectrometer (ICP-MS) allows simultaneous measurement of an array of other element to calcium ratios on the same sample, including temperature-sensitive Mg/Ca ratios. This proxy may therefore have the potential to generate temporally and spatially high resolution paleo-CO_2 reconstructions to better characterize climate sensitivity.

Based on core-top calibrations of the B distribution coefficient "K_D" (see below) against seawater temperature, several studies reproduced glacial–interglacial CO_2 fluctuations comparable to ice core records based on B/Ca of planktonic foraminifers (Yu et al., 2007, 2013). Moreover, a recent study of a Pacific deep sea core by Penman et al. (2014) indicated an abrupt decrease in both B/Ca and $\delta^{11}B$ of planktonic foraminifers in concert with the characteristic 3–4‰ negative carbon isotope ($\delta^{13}C$) excursion of the Paleocene-Eocene Thermal Maximum (~56 Myr: Kennett and Stott, 1991; Zachos et al., 2001). The records were interpreted as evidence for an ocean acidification episode in response to massive carbon input into the ocean–atmosphere system, which is consistent with sedimentological and modeling constraints (Zachos et al., 2005; Zeebe et al., 2009; Uchikawa and Zeebe, 2010). For benthic foraminifers, core-top data provide robust calibration against $\Delta[CO_3^{2-}]$, where $\Delta[CO_3^{2-}] = [CO_3^{2-}]_{In\ Situ} - [CO_3^{2-}]_{Saturation}$ (Yu and Elderfield, 2007; Brown et al., 2011; Rae et al., 2011; Raitzsch et al., 2011; Yu et al., 2013). Since the pioneering down-core application by Yu and Elderfield (2007), this calibration has been utilized to assess the efficiency of physical and biogeochemical carbon transport between the atmosphere and deep ocean reservoir over glacial–interglacial timescales (Rickaby et al., 2010; Yu et al., 2010; Doss and Marchitto, 2013; Yu et al., 2013; Yu et al., 2014). Though these studies showcased remarkable potential, precise controls on the B/Ca proxy are still under debate. Allen and Hönisch (2012) argued that the apparent relationship between K_D and temperature may be due to the natural co-variation of temperature with carbonate chemistry and other environmental parameters. In addition, B/Ca of planktonic foraminifers from core-top and culture studies show varying degrees of apparent species-specific dependence on multiple physicochemical parameters and possibly kinetic effects related to growth rates (Sanyal et al., 1996; Wara et al., 2003; Ni et al., 2007; Foster, 2008; Allen et al., 2011, 2012; Yu et al., 2013).

The difficulties in filling such gaps in understanding arise from several reasons. Firstly, many of the physicochemical parameters co-vary in seawater, making it challenging to isolate the individual influence of a given parameter. For instance, a shift in seawater pH usually causes simultaneous changes in the speciation of dissolved B and dissolved inorganic carbon (DIC) species, $CaCO_3$ saturation state, and precipitation rate (R). Secondly, the chemistry of the fluid reservoir for calcification often deviates from ambient seawater due to biological processes carried out by the foraminifers and/or algal symbionts (Rink et al., 1998; Bentov et al., 2009; de Nooijer et al., 2009), which are collectively called vital effects. Hönisch et al. (2003) observed a clear dependence of $\delta^{11}B$ of symbiont-bearing *Orbulina universa* on light availability, which modulates the net photosynthesis/respiration balance. This in turn alters carbonate and B chemistry of the microenvironment surrounding the calcifying shell (Rink et al., 1998; Wolf-Gladrow et al., 1999; Zeebe et al., 2003).

These impediments can be minimized in carefully controlled inorganic experiments. There are a few cases where measurements of B contents are reported for $CaCO_3$ synthesized from B-bearing fluids (Kitano et al., 1978; Hemming et al., 1995; Hobbs and Reardon, 1999; Sanyal et al., 2000; He et al., 2013; Gabitov et al., 2014b), and the relevant results indicate that B contents in $CaCO_3$ increase with pH and total B concentration (denoted as $[B_T]$, where $[B_T] = [B(OH)_3] + [B(OH)_4^-]$) of the parent fluids. Nevertheless, these two variables alone are insufficient to disentangle the intertwined dissolved B chemistry and carbonate chemistry parameters and to explicitly identify what ultimately governs B/Ca in $CaCO_3$. The objective of the present study is to perform laboratory experiments to advance our understanding of the B incorporation mechanism and the fundamental basis of the B/Ca proxy. To this end, we performed a suite of inorganic calcite precipitation experiments based on a seeded overgrowth technique using a pH-stat system. Unlike previous studies, we systematically varied pH, $[B_T]$, [DIC] (where $[DIC] = [CO_{2(aq)}] + [HCO_3^-] + [CO_3^{2-}]$), and $[Ca^{2+}]$ in our experiments.

2. THEORETICAL BACKGROUND

Dissolved B in solutions exists as trigonally-coordinated $B(OH)_3$ and tetrahedrally-coordinated $B(OH)_4^-$. Their relative abundance is pH-sensitive such that $B(OH)_3$ dominates at lower pH while $B(OH)_4^-$ dominates at higher pH (Fig. 1A):

$$B(OH)_3 + H_2O \leftrightarrow B(OH)_4^- + H^+ \quad (1)$$

Due to the differences in molecular geometries and vibrational frequencies, $B(OH)_3$ is more enriched in ^{11}B isotopes relative to $B(OH)_4^-$ (Kakihana et al., 1977; Liu and Tossell, 2005; Zeebe, 2005; Klochko et al., 2006). This results in a constant $\delta^{11}B$ offset of 27.2‰ between $B(OH)_3$ and $B(OH)_4^-$ at equilibrium (Klochko et al., 2006). Given that the $\delta^{11}B$ value of B_T in modern seawater is constant at 39.6‰ (Foster et al., 2012), the isotopic compositions of $B(OH)_3$ and $B(OH)_4^-$ are also a function of pH

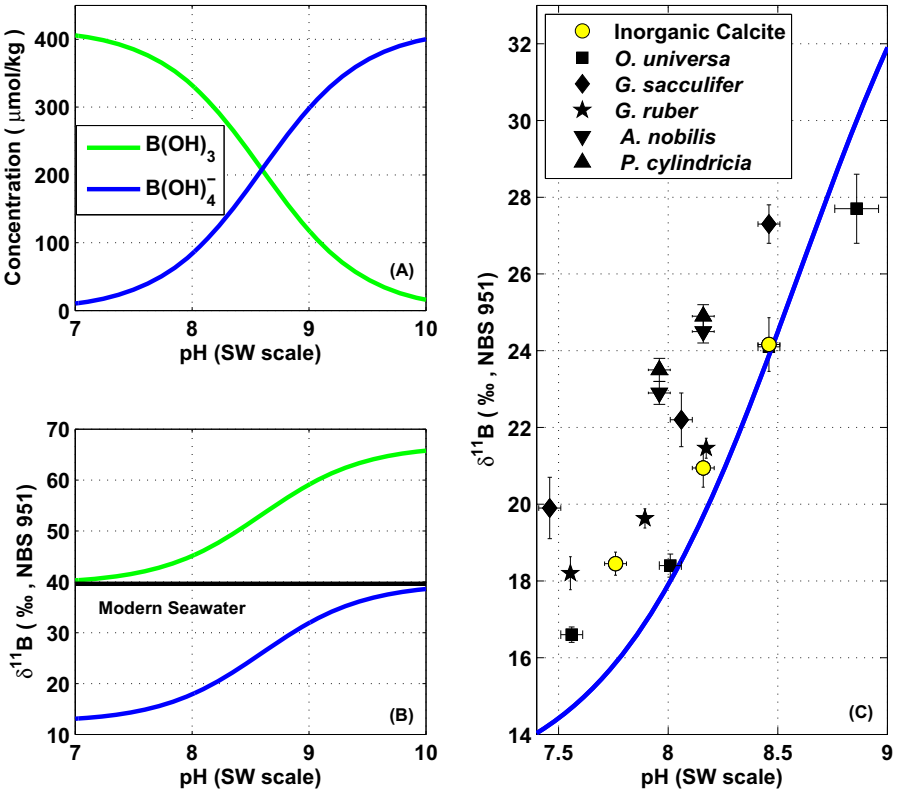

Fig. 1. Concentration (Panel A) and $\delta^{11}B$ (Panel B) of $B(OH)_3$ and $B(OH)_4^-$ as a function of pH at temperature = 25 °C and salinity = 35 (practical salinity units). The chemical and isotopic system are calculated for the typical seawater concentration and the modern $\delta^{11}B$ value of B_T (416 μmol/kg and 39.61‰) using $pK_B = 8.60$ and equilibrium $B(OH)_3$–$B(OH)_4^-$ isotope fractionation factor of 1.0272 (Dickson et al., 2007; Klochko et al., 2006; Foster et al., 2010). (Panel C) Empirical $\delta^{11}B$–pH relationships of synthetic and biogenic $CaCO_3$ juxtaposed against predicted $\delta^{11}B$ values of $B(OH)_4^-$ as a function of pH. Original pH data are adjusted to the seawater scale here if necessary. Data source: Inorganic calcite (Sanyal et al., 2000), *Orbulina universa* (Sanyal et al., 1996), *Globigerinoides sacculifer* (Sanyal et al., 2001), *Globigerinoides ruber* (Henehan et al., 2013), *Acropora nobilis* and *Porites cylindrica* (Hönisch et al., 2004).

(Fig. 1B). Vengosh et al. (1991) and Hemming and Hanson (1992) showed that $\delta^{11}B$ values of modern marine carbonates fall within a relatively narrow range that is similar to the $\delta^{11}B$ values of $B(OH)_4^-$ in seawater. They hence postulated that $B(OH)_4^-$ is primarily incorporated into carbonates. Close agreement between $\delta^{11}B$ values of biogenic and synthetic $CaCO_3$ and those of $B(OH)_4^-$ has been verified in subsequent culture and inorganic experiments (Sanyal et al., 1996, 2000, 2001; Hönisch et al., 2004; Henehan et al., 2013), which is summarized in Fig. 1C. Furthermore, it has been experimentally demonstrated that B contents in synthetic $CaCO_3$ increase with solution pH and $[B_T]$ (Hemming et al., 1995; Sanyal et al., 2000; He et al., 2013). Raising $[B_T]$ at a constant pH (Hemming et al., 1995) causes both $[B(OH)_3]$ and $[B(OH)_4^-]$ to increase, whereas raising pH at a constant $[B_T]$ (Sanyal et al., 2000; He et al., 2013) causes only $[B(OH)_4^-]$ to increase but $[B(OH)_3]$ to decrease. These results have been considered as the key supporting evidence for selective B incorporation via $B(OH)_4^-$.

Hemming and Hanson (1992) hypothesized that B incorporation in $CaCO_3$ can be summarized as:

$$CaCO_3 + B(OH)_4^- \rightarrow Ca(HBO_3) + HCO_3^- + H_2O \qquad (2)$$

For the substitution reaction, the fluid-$CaCO_3$ B distribution coefficient "K_D" may be expressed as (Hemming and Hanson, 1992; Yu et al., 2007):

$$K_D = \frac{\left(\frac{[HBO_3^{2-}]}{[CO_3^{2-}]}\right)_{CaCO_3}}{\left(\frac{[B(OH)_4^-]}{[HCO_3^-]}\right)_{Fluid}} \cong \frac{(B/Ca)_{CaCO_3}}{\left(\frac{[B(OH)_4^-]}{[HCO_3^-]}\right)_{Fluid}} \qquad (3)$$

Wara et al. (2003) and Yu et al. (2007) noted a covariance in planktonic foraminiferal B/Ca and Mg/Ca ratios in their core-top dataset, which fueled the attempts to calibrate K_D against seawater temperatures. If the correlation between K_D and temperature were robust, it follows that seawater $[B(OH)_4^-]/[HCO_3^-]$ ratios could be derived from paired B/Ca and Mg/Ca measurements by ICP-MS. The $[B(OH)_4^-]/[HCO_3^-]$ ratios could then be used to constrain the ocean CO_2 system with an additional carbonate chemistry parameter such as alkalinity or pH (*e.g.*, Yu et al., 2007, 2013; Foster, 2008). However, temperature variations imposed hardly any influence on K_D for cultured planktonic foraminifers (Allen et al., 2012). Moreover, *O. universa* cultured under a constant temperature resulted in variable K_D values in pH, $[B_T]$ and salinity manipulations (Sanyal et al.,

1996; Allen et al., 2011). This suggests that factors besides temperature may also influence B incorporation and K_D. Allen and Hönisch (2012) also argued that the correlation between K_D and temperature based on core-top calibrations potentially reflects a mathematical artifact driven by the denominator (Eq. (3)), and cautioned the down-core applications.

The mode of B incorporation described in Eq. (2) (Hemming and Hanson, 1992) implies initial adsorption of $B(OH)_4^-$ onto the $CaCO_3$ surfaces and subsequent substitution of the CO_3^{2-} anion groups in $CaCO_3$ with HBO_3^{2-}, which requires a tetrahedral to trigonal coordination change. But this view is controversial. Using ^{11}B MAS NMR spectroscopy, Sen et al. (1994) reported that B in calcite and aragonite exists in trigonal and tetrahedral form, respectively. This suggests that aragonite should be more compatible with B as no coordination change is required, which seems to agree with generally higher B contents in aragonite than in calcite (Hemming and Hanson, 1992; Sinclair et al., 1998; Allison et al., 2010). However, Klochko et al. (2009) later published contrasting evidence of nearly equal abundance of trigonal and tetrahedral B in calcite and aragonite. Tossell (2006) and Klochko et al. (2009) argued that the detection of purely trigonal B in calcite by Sen et al. (1994) can be due to a miscounting of ^{11}B MAS NMR spectra of the $B(OH)_2CO_3^-$ as $B(OH)_3$. Ruiz-Agudo et al. (2012) performed nano-scale observations using atomic force microscopy and argued that B may reside in non-lattice (defect) sites in calcite under certain circumstances. They also commented that the balance between the rate of $CaCO_3$ precipitation and of B coordination change may be an important factor. They argued there would be sufficient time for coordination change at slower growth rates, which should enhance the stability and overall B contents in $CaCO_3$. However, recent experimental evidence suggests the opposite. Gabitov et al. (2014b) synthesized calcite using a free drift technique where crystal growth rate varied over time. The resultant crystals had internal B heterogeneity in such a way that B abundances increase with linear growth rates in different crystal sections.

In summary, extensive research in recent years has generated intriguing yet in some cases conflicting discoveries. The available evidence points to the need of additional dimensions in the present theoretical framework of the B/Ca proxy proposed by Hemming and Hanson (1992), for which a better understanding of the crucial abiotic factors for B incorporation is required.

3. METHODS

3.1. Experimental set-up and seeded $CaCO_3$ overgrowth technique

Fig. 2 shows the pH-stat system used in this study. The air-tight acrylic reaction chamber has ports for titrant input and calcite seed addition. The chamber immersed in a 25 °C water bath was connected to a titrator system via a pH electrode (Thermo Scientific #8165BNWP), which was calibrated by NIST pH buffers before each experiment. The titrator system received voltage readings from the electrode every second and logged pH (NBS scale) by averaging the signals over a 10 s-interval. The system was set to dose titrants through a gas-impermeable tube upon a 0.01 unit of pH deviation from assigned values. Titrants (0.3 M NaOH and ^{13}C-spiked Na_2CO_3 solutions; see below) were prepared and sealed into 15 mL HDPE serum vials under N_2 atmosphere in a glove-bag.

The seeded calcite overgrowth technique was modified from Sanyal et al. (2000) and Zeebe and Sanyal (2002). A key feature of this technique is that the parent fluids were saturated with respect to calcite, yet the extent of saturation was insufficient to trigger spontaneous nucleation unless the seeds were introduced. The seeds provided the reactive surfaces for new $CaCO_3$ to nucleate and grow. In essence, the role of the seeds here is analogous to that of foraminiferal organic matrices in providing initial nucleation templates for calcification (also see Zeebe and Sanyal, 2002). The overgrowth technique has key practical merits. The mineralogy of the seeds typically determines that of the overgrowth. For example, calcite seeds induce calcite overgrowth (and so does aragonite) regardless of the fluid

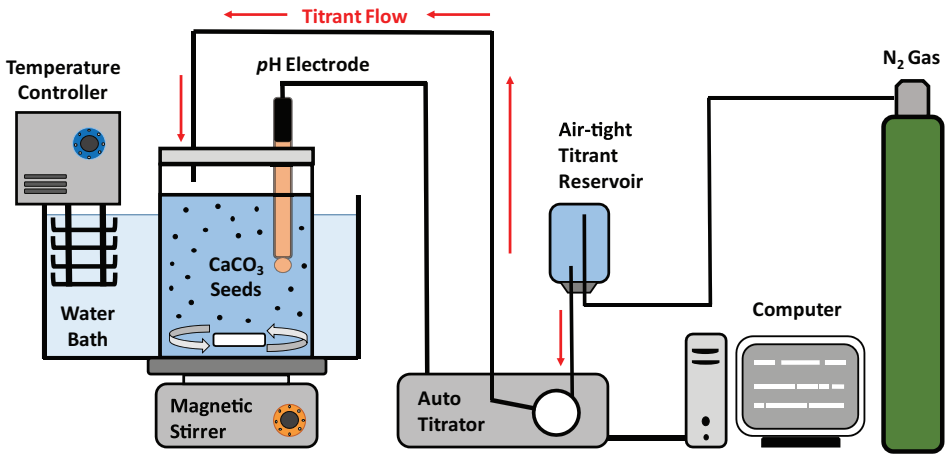

Fig. 2. Illustration of the experimental set-up.

chemistry such as the presence/concentration of Mg^{2+} (*e.g.*, Romanek et al., 1992; Zeebe and Sanyal, 2002). This is crucial as B seems to have distinct compatibility with synthetic calcite and aragonite (Kitano et al., 1978; Hemming et al., 1995). We used 10-micron calcite seeds (Sigma–Aldrich #310034), which (1) contained no other $CaCO_3$ polymorphs, (2) were essentially free of B (B/Ca = 1.01 ± 1.65 μmol/mol, 1σ S.D., $n = 5$), and (3) were isotopically homogeneous ($\delta^{13}C = -18.59 \pm 0.07‰$, $\delta^{18}O = -21.10 \pm 0.04‰$, 1$\sigma$ S.D., $n = 5$).

The general expression of $CaCO_3$ precipitation may be written as:

$$Ca^{2+} + 2HCO_3^- \leftrightarrow CaCO_3 + CO_2 + H_2O \quad (4)$$

Precipitation of $CaCO_3$ thus lowers fluid pH and concurrently lowers alkalinity and [DIC] in 2:1 ratio. These changes were balanced by the Na_2CO_3 titrant to maintain the carbonate chemistry at near-constant state. It should be noted that the stock Na_2CO_3 solutions for the titrant and parent fluids were ^{13}C-spiked to $\delta^{13}C_{VPDB} = +400‰$ or +606.8‰. New layers of calcite overgrowth thus acquired B as well as highly ^{13}C-enriched signature from the parent fluids. We used the $\delta^{13}C$ constraint to calculate B/Ca in the overgrowth fraction (see below). In theory, the overgrowth fraction can be quantified by simply weighing the final sample yield and initial seed mass (*e.g.*, Sanyal et al., 2000). However, we encountered sporadic accidental spill and loss of material during filtration in our preliminary experiments. The ^{13}C-spike provided an independent and more consistent constraint for the overgrowth fraction even upon mishandling during filtration.

3.2. Experimental procedures

Solutions (1 L) of NaCl–$CaCl_2$–$B(OH)_3$–Na_2CO_3 were used as the parent fluids. We used Milli-Q ultra-pure deionized H_2O that was continuously bubbled with N_2 gas in advance (*i.e.*, CO_2-free H_2O) for the parent fluids. We also avoided the use of borosilicate glassware to minimize the risk of B contamination (Green et al., 1976).

The parent fluids were prepared as follows. First, NaCl and $B(OH)_3$ were dissolved in ~850 mL of H_2O in a 1 L plastic volumetric flask, to which 1 M $CaCl_2$ and a small amount of 1 M HCl stock solutions were added. After purging the headspace with N_2 and mixing, the solution was kept in the water bath overnight. In a separate 100 mL plastic volumetric flask, Na_2CO_3 solution was prepared to a desired [DIC] by diluting the ^{13}C-spiked 0.3 M Na_2CO_3 stock solutions in a N_2-filled glove-bag. A small amount of HCl was also added for pH adjustment. Second, the latter solution was mixed into the former solution and the final volume was brought up to 1 L by H_2O. The mixture was sealed into the reaction chamber and kept in the water bath for 1 h. Then the parent fluid was titrated with 0.3 M NaOH to a desired pH and allowed to equilibrate for ~2 h (Fig. 3A and B).

Once the solution pH was fully stabilized (*i.e.*, chemically equilibrated), the titrant was switched from NaOH to the ^{13}C-spiked 0.3 M Na_2CO_3 solution. After monitoring the pH for additional 10 min, 80 mg of the seeds were introduced to initiate calcite overgrowth (Fig. 3A and B). The progress of the overgrowth was monitored by the volume of titrant addition. Experiments were normally terminated after nearly doubling of calcite in mass due to the overgrowth. The samples were collected onto 0.2 μm membrane filters and rinsed rigorously with H_2O. They were subsequently dried at 65 °C, weighed for the total mass, and stored until $\delta^{13}C$ and B/Ca measurements. After each experiment, the chamber was cleaned with non-abrasive sponge, soaked in 10% HCl and thoroughly rinsed with H_2O.

We systematically modified pH, $[B_T]$, [DIC] and $[Ca^{2+}]$ of the parent fluids (Table 1). The rational for each set of experiments is as follows. The pH and $[B_T]$ variation experiments were conducted to further validate previously reported B/Ca dependence on these parameters in inorganic and foraminiferal calcite (Hemming et al., 1995; Sanyal et al., 1996; Hobbs and Reardon, 1999; Sanyal et al., 2000; Allen et al., 2011, 2012; He et al., 2013). The pH variation experiments were repeated at three different $[B_T]$ for comparison with Sanyal et al. (2000) and He et al. (2013), who performed analogous pH variation experiments at relatively high $[B_T]$. The [DIC] variation experiments were designed to test if the negative correlation between [DIC] and B/Ca of cultured planktonic foraminifer *Globigerinoides sacculifer* (Allen et al., 2012) can be similarly observed in inorganic calcite. The $[Ca^{2+}]$ variation experiments were intended to assess the effect of precipitation rate on B incorporation in calcite, as changing $[Ca^{2+}]$ exerts significant control on calcite saturation and precipitation rate but negligible changes in the DIC and B speciation. Finally, we performed an additional set of experiments where pH and $[Ca^{2+}]$ were jointly varied at a fixed calcite saturation in order to maintain a relatively constant precipitation rate R at two different pH and $[Ca^{2+}]$ combinations. Individual experiments were typically repeated in triplicate. Chemical manipulations for the experimental series and their effects on fluid chemistry with respect to the control are summarized in Table 1.

We used the aqueous geochemical model PHREEQC (Parkhurst and Appelo, 1999) in conjunction with WATEQ4 thermodynamic database (Ball and Nordstrom, 1991) to constrain fluid chemistry and calcite saturation index ($SI_{Calcite}$), which is defined as:

$$SI_{Calcite} = \log_{10} Q/K_{SP} \quad (5)$$

where Q is Ca^{2+} and CO_3^{2-} ion activity product and K_{SP} is the thermodynamic calcite solubility product ($=10^{-8.48}$ at 25 °C: Plummer and Busenberg, 1982). A more practical measure of calcite saturation for oceanographic practices would be the saturation state $\Omega_{Calcite}$, which is defined as the quotient of in-situ total Ca^{2+} and CO_3^{2-} concentration divided by the stoichiometric solubility product K^*_{SP}. Because K^*_{SP} depends on solution chemistry, if we are to report $\Omega_{Calcite}$ properly, K^*_{SP} values that are specific to individual experimental conditions need to be determined independently. This is the reason why $SI_{Calcite}$ values are reported here. The PHREEQC program derives activity coefficients by the Davies equation. The dissociation constants for dissolved B and DIC species in WATEQ4 are from Mesmer et al. (1972) and Plummer and Busenberg (1982), respectively. See Table S1 (Supplementary materi-

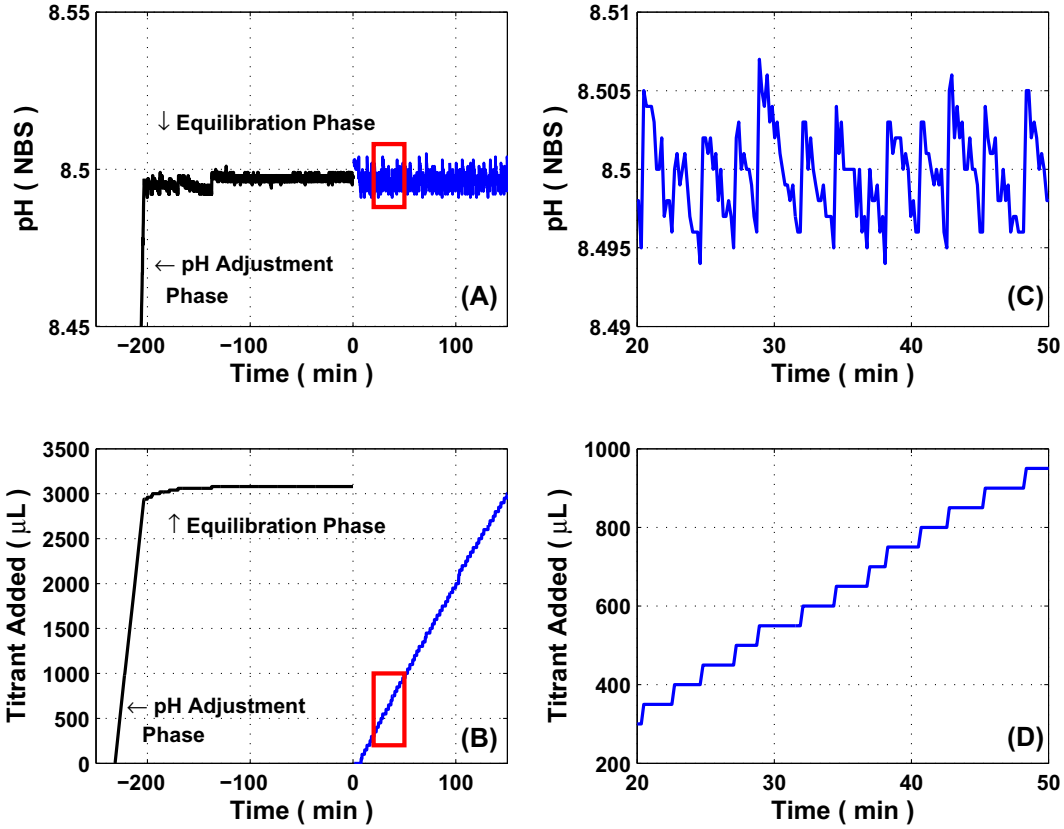

Fig. 3. Typical titration sequence of the parent fluid preparation (black) and overgrowth experiment (blue). Experiment 6C is used as an example here. (Panels A and B) During the preparation, parent fluid was titrated with NaOH to a desired pH value and subsequently equilibrated for ~2 h. Time zero marks the seed addition and the start of the calcite overgrowth phase, during which the system was titrated with ^{13}C-spiked Na_2CO_3. (Panels C and D) Close-up view of the red rectangle shown in Panels A and B. Calcite precipitation lowers pH, total alkalinity and [DIC] of the parent fluid (Eq. (4)). These were compensated for by Na_2CO_3 titrant. A minor "jump" in the titrant dosing log at ~100 min (Panel B) indicates a lag-time, during which the internal 2 mL titrant reservoir had to be refilled from the external reservoir (see Fig. 2). This jump does not indicate a sudden change in the pacing of titrant addition. (For interpretation of the references to colour in this figure legend, the reader is referred to the web version of this article.)

als) for detailed information on fluid chemistry for all experiments.

3.3. Mass balance calculations

We employed the following double mass-balance equations to calculate B/Ca in the calcite overgrowth:

$$\delta^{13}C_{Sample} = (f_{OG}) \times (\delta^{13}C_{OG}) + (1 - f_{OG}) \times (\delta^{13}C_{Seeds}) \quad (6)$$

$$(B/Ca)_{Sample} = (f_{OG}) \times ((B/Ca)_{OG}) + (1 - f_{OG}) \times ((B/Ca)_{Seeds}) \quad (7)$$

where f_{OG} refers to the overgrowth mass fraction with respect to the final (total) sample mass. The $\delta^{13}C_{OG}$ value in Eq. (6) can be derived from the ^{13}C-spike of the stock Na_2CO_3 solutions and carbon isotope fractionation factor between calcite and DIC ($\varepsilon_{Calcite\text{-}DIC}$). HCO_3^- was by far the most dominant DIC species in the parent fluids. We thus applied the fractionation factor of $\varepsilon_{Calcite\text{-}HCO_3^-} = 1.0 \pm 0.2‰$ by Romanek et al. (1992), which is largely independent of temperature and precipitation rate R. The $\delta^{13}C_{OG}$ value can be calculated as +401.4‰ and 608.4‰ for the ^{13}C-spike of +400‰ and +606.8‰. Eq. (6) can then be solved for f_{OG}, which feeds into Eq. (7) to solve for B/Ca in the overgrowth fraction denoted as $(B/Ca)_{OG}$.

Due to pH-dependent DIC speciation, the $\delta^{13}C$ value of HCO_3^- ($\delta^{13}C_{HCO_3}$) within the DIC pool of a given isotopic composition can vary by a few ‰ (see Fig. 3.2.14 in Zeebe and Wolf-Gladrow, 2001). For the pH range between 8 and 9, which encompasses all of our experiments, the $\delta^{13}C_{HCO_3}$ value may vary by ~1‰ at most. Thus, we assigned an uncertainty of ±1‰ in the $\delta^{13}C_{OG}$ estimates for the error propagation. But this factor is fairly insignificant. The mass-balance equations show that, even if $\varepsilon_{Calcite\text{-}DIC}$ value varies by as much as ±3‰, the $(B/Ca)_{OG}$ error can be contained within 1% for the ^{13}C-spike applied here (see Fig. S1 in Supplementary materials).

3.4. Analytical methods

Aliquots of the samples for the $\delta^{13}C$ and B/Ca measurements were homogenized using a mortar and pestle. The mortar and pestle were cleaned with methanol before/after each sample to avoid cross-contamination. Approximately 60 µg and 300 µg of the homogenized samples were analyzed for $\delta^{13}C$ and B/Ca, respectively.

The $\delta^{13}C$ analyses were performed at the UC Santa Cruz (UCSC) Stable Isotope Laboratory on a ThermoFinnegan

Table 1
A summary of chemical manipulations and consequent changes in the distributions of the dissolved B and DIC species as well as calcite saturation index relative to the control.

	pH (NBS scale)	[DIC] (μmol/kg)	$[B_T]$ (μmol/kg)	$[Ca^{2+}]$ (μmol/kg)	Calcite Sat. Index
Control	8.25	2393	432	3851	0.54
Experimental series	Varied parameter(s)	Constant parameters	B speciation	DIC speciation	Calcite Sat. Index
pH Exp.	pH pH = 8.0, 8.37, 8.5 & 8.65.	$[B_T]$ [DIC] $[Ca^{2+}]$	Varies	Varies	Varies
pH Exp. @ $5 \times [B_T]_{Ctrl}$	pH & $[B_T]$ pH = 8.25, 8.5 & 8.75 @ $[B_T]$ = 2184 μmol/kg	$[B_T]$ [DIC] $[Ca^{2+}]$	Varies	Varies	Varies
pH Exp. @ $10 \times [B_T]_{Ctrl}$	pH & $[B_T]$ pH = 8.0, 8.25, 8.5 & 8.75 @ $[B_T]$ = 4317 μmol/kg	$[B_T]$ [DIC] $[Ca^{2+}]$	Varies	Varies	Varies
B Exp.	$[B_T]$ $[B_T]$ = 864, 2184 & 4317 μmol/kg	pH [DIC] $[Ca^{2+}]$	Varies	≈Control	≈Control
DIC Exp.	[DIC] [DIC] = 1795, 3589 & 4787 μmol/kg	pH $[B_T]$ $[Ca^{2+}]$	≈Control	Varies	Varies
Ca Exp.	$[Ca^{2+}]$ $[Ca^{2+}]$ = 4817, 5778 & 7706 μmol/kg	pH $[B_T]$ [DIC]	≈Control	≈Control	Varies
pH & Ca Exp.	pH & $[Ca^{2+}]$ @ pH = 8.37 & $[Ca^{2+}]$ = 2978 μmol/kg @ pH = 8.0 & $[Ca^{2+}]$ = 6796 μmol/kg	$[B_T]$ [DIC]	Varies	Varies	≈Control

MAT 253 dual-inlet isotope ratio mass spectrometer coupled to a Kiel IV carbonate device. Reproducibility of the $\delta^{13}C$ analysis was ±3.2‰ on average (1σ S.D. of the duplicate runs for all samples), which is much higher than the usual reproducibility reported for carbonate standards (1σ S.D. = ~±0.1‰). This lower precision is likely due to the fact that our synthetic calcite samples were extremely enriched in ^{13}C relative to the standards, reference gas, and natural samples ($\delta^{13}C = -10$ to +10‰) routinely measured on this instrument. Using standard dual-inlet techniques, isotopic ratio measurement alternates between sample gas and reference gas, which has a natural (non-enriched) $\delta^{13}C$ value. Small amounts (<1% of sample size) of sample-reference gas mixing may occur over these cycles. This mixing within the dual inlet sample introduction system is tolerable if samples and reference gas have similar $\delta^{13}C$ values, however, when they differ by ~200‰ as in this study, even a small amount of mixing (especially if it is variable) may have a significant negative effect on precision. Precision could likely be improved by measuring samples relative to a reference gas that is more similar to samples (~200‰). However, the reduced precision we encountered does not compromise the reliability in the final estimates for $(B/Ca)_{OG}$, which is dominated by the uncertainty in the B/Ca analysis. As described above, $\delta^{13}C$ error of ~3‰ would impose only 1% of error in $(B/Ca)_{OG}$ (Fig. S1). Analysis of non-enriched standards immediately after ^{13}C-spiked samples showed no sample-to-sample memory effect from sample handling, sample dissolution and CO_2 separation in the Kiel device, or $\delta^{13}C$ measurement in the mass spectrometer.

The B/Ca analyses were performed at the UCSC Marine Analytical Laboratory on a Thermo Element XR ICP-MS following the methods of Brown et al. (2011). Homogenized samples were dissolved in 800 µL of 0.075 N HNO_3 prepared with Optima-grade acid and B-clean Milli-Q H_2O (produced using Q-gard B purification pack). Blanks were measured every 5 samples (and more frequently for samples with high B contents, see below) on the same HNO_3 used to dissolve the samples. B blank reduction and consistency was achieved by long take-up and washout times (30 s and 40 s, respectively) as well as injecting NH_3 gas into the spray chamber at 5 mL/min, a technique developed to reduce B blanks by raising spray chamber droplet pH to convert $B(OH)_3$ into non-volatile $B(OH)_4^-$ (Al-Ammar et al., 1999; Foster, 2008). Calibration was performed by measuring a suite of standards prepared with Certi-Prep elemental standards mixed to a range of B/Ca ratios, and diluted on the day of each analytical session to varying $[Ca^{2+}]$ across the range of 40–200 ppm. No effect of varying $[Ca^{2+}]$ on calibration was detected, and all samples were run at a $[Ca^{2+}]$ within the range of our standards. A liquid consistency standard was run every 5 samples to monitor and correct for in-run drift.

The methods of Brown et al. (2011) are optimized for natural foraminiferal samples, which typically have B/Ca of 30–200 µmol/mol. Yet, some of our samples had much higher B contents up to ~1500 µmol/mol, which required us to establish a new set of standards and a careful control on the sample/blank sequence for ICP-MS runs. New standards were mixed to produce calibration curves (B/Ca = 500, 1000 and 2000 µmol/mol) that encompassed the range of pre-determined sample B/Ca values from preliminary runs. The relationship between measured and known B/Ca remained linear across the range measured. A significant B memory effect was observed following the measurements of samples with high B contents (>~500 µmol/mol). This was dealt with by two strategies. First, where reasonable predictions could be made from experimental conditions (*e.g.*, samples synthesized at elevated $[B_T]$ and/or pH were expected to have higher B/Ca), the sequence of an analytical run was ordered so that the samples predicted to have relatively low B/Ca were measured before the ones with higher B contents. Second, all samples predicted to have B/Ca higher than ~500 µmol/mol were bracketed by 2 or in some cases 3 blanks (essentially adding 4 min of washout time per blank) to ensure that the blank immediately preceding each sample measurement was within background levels.

Sample B/Ca values are based on a single measurement. The long-term precision of the B/Ca analysis was determined by repetitive measurements of the consistency standard, found to be ±2.2% or ±1.6 µmol/mol (1σ S.D., $n = 46$) during the course of several analytical sessions over more than a year. Repeat analyses of two samples demonstrated similar variance to that of the consistency standard (Sample 1A: average B/Ca = 629 µmol/mol, 1σ S.D. = 12.8 µmol/mol or 2.2%, $n = 6$, and Sample 17C: average B/Ca = 76.2 µmol/mol, 1σ S.D. = 1.9 µmol/mol or 2.5%, $n = 11$), confirming that the precision of consistency standard measurements is representative of the external precision on samples. The larger of the percentage (2.2%) or the absolute value (±1.6 µmol/mol) was assigned as the B/Ca analytical uncertainty for all samples.

As a test for the presence of surface-adsorbed B or other contaminants not removed by post-filtration rinsing, several samples across a range of B/Ca were cleaned using the trace-metal foraminiferal cleaning procedures of Barker et al. (2003), which involves several sonication and rinsing steps in methanol and B-free Milli-Q as well as an oxidative and reductive step. Comparison of B/Ca results between cleaned and un-cleaned aliquots show that they fall about a 1:1 line (Fig. S2), suggesting that the post-filtration rinsing of the samples is sufficient to remove all surface-adsorbed B that is not fully incorporated into calcite. We hence did not apply the cleaning step for all B/Ca measurements. Some non-systematic scatter is observed in comparison of cleaned and un-cleaned samples (Fig. S2). This is probably due to the very high sample loss (50–90%) during cleaning of inorganic calcites, which have a very fine grain size and slow settling velocities.

The uncertainty for the calculated $(B/Ca)_{OG}$ values represents 2σ standard deviation (95% confidence interval), for which the uncertainties associated with the $\delta^{13}C$ and B/Ca analyses on the samples and initial calcite seeds (see above) as well as the uncertainty of ±1‰ on the $\delta^{13}C_{OG}$ estimates due to the pH effect (see Section 3.3) were propagated. The B/Ca values reported hereafter refer to the $(B/Ca)_{OG}$. As

the margin of error for the average B/Ca value for a given experiment, we report 1σ standard deviation based on the results from replicate experiments (usually $n = 3$).

4. RESULTS

All experimental data are listed in Table S1 (Supplementary materials). Inspections by X-ray diffraction and scanning electron microscopy reveal that samples collected after the overgrowth phase retained the original calcite mineralogy and rhombohedral crystal structure of the starting seeds (Fig. S3). The estimates for the overgrowth mass fraction by $\delta^{13}C$ mass-balance and by weighing agreed within ±5% (Fig. S4). The mass of the overgrowth was typically on the order of 65–95 mg, accounting for 45–55% of the total mass of the samples (*i.e.*, doubling of the initial seed mass).

Changes in carbonate chemistry from $CaCO_3$ precipitation (Eq. (4)) were compensated for by titration with Na_2CO_3. But this was not the case for Ca^{2+} drawdown. Calculations suggest that roughly 10–25% of Ca^{2+} had to be withdrawn from the parent fluids to yield ~80 mg of calcite overgrowth (the loss was ~20% for the majority of the experiments conducted at $[Ca^{2+}]$ equal to that of the control), however, we observed hardly any change in the pace of titrant addition over the course of each experiment (see Fig. 3 for example). This implies that a relatively constant precipitation rate R was maintained despite Ca^{2+} drawdown during an experiment. It is likely that the negative impact of continuous Ca^{2+} depletion on R was mitigated by concurrent increase in the surface area of calcite crystals over the course of each experiment (see below).

We report R on a logarithmic scale in the unit of mol/m^2/s using the quantity of calcite overgrowth (based on ^{13}C mass-balance) precipitated during the experimental duration. Assuming cubic shape of individual crystals and calcite density of 2.7×10^6 g/m^3, the surface area of the 10-micron seeds per unit mass can be estimated as is $6/(10 \times 10^{-6}\ m)/(2.7 \times 10^6\ g/m^3) = 0.22\ m^2/g$ (Zeebe and Sanyal, 2002). It follows that the total surface area provided by 80 mg of calcite seeds at the beginning of the experiments is 0.018 m^2. But this value changes with time as the individual crystals grow in size due to the overgrowth. For example, the total surface area will increase to 0.028 m^2 upon doubling in the mass of calcite crystals (*i.e.*, $f_{OG} = 0.5$). This leads to $\log_{10}R$ variations of 0.01–0.02 for a given amount of overgrowth and experimental duration. We used the average total surface area over the course of the experiments, hence the R values reported here indicate the time-averaged rates. The uncertainty for the $\log_{10}R$ values represents 2σ standard deviation, which is based on the $\delta^{13}C$ analytical uncertainty as well as ±1‰ of uncertainty in the $\delta^{13}C_{OG}$ estimates (see Section 3.3). The margin of error for the average $\log_{10}R$ value for a given experiment is given as 1σ standard deviation based on the results from replicate experiments.

Calculated $\log_{10}R$ varied from −6.59 to −5.15, generally in accordance with $SI_{Calcite}$ (Fig. S5). Consequently, we observed positive correlations between R and pH, [DIC] and $[Ca^{2+}]$ when everything else besides these parameters was held constant (Fig. 4A, B, D and E). In contrast, the relation between R and $[B_T]$ was not so systematic (Fig. 4C). A doubling in $[B_T]$ from the control ($[B_T]_{Ctrl} = 432$ μmol/kg) resulted in subtle increase in $\log_{10}R$ from -5.72 ± 0.03 to -5.58 ± 0.04, yet further increase in $[B_T]$ to 2184 and 4317 μmol/kg caused $\log_{10}R$ to decrease (-5.62 ± 0.02 and -5.81 ± 0.03). A similar response of R to $[B_T]$ variations was documented at pH 8.5 based on the samples from three sets of the pH variation experiments performed at $[B_T]_{Ctrl}$, $5\times[B_T]_{Ctrl}$ and $10\times[B_T]_{Ctrl}$. In the last set of experiments where pH and $[Ca^{2+}]$ were jointly varied at a fixed $SI_{Calcite}$, relatively constant R was achieved at two pH and $[Ca^{2+}]$ combinations (see Fig. 4E and F).

Fig. 5 displays the effect of chemical manipulations on B/Ca. Six replicate experiments were made for the control. The average B/Ca for the control was 28.4 ± 7.5 μmol/mol. Calcite precipitated from the parent fluids adjusted to pH 8.00 was essentially B-free ($B/Ca = 0.8 \pm 0.3$ μmol/mol, Fig. 5A). In contrast, B/Ca increased systematically when the fluid pH was raised. As shown in Fig. 5B, an increasing trend in B/Ca with pH was also evident at elevated $[B_T]$ levels (at $5\times[B_T]_{Ctrl}$ and $10\times[B_T]_{Ctrl}$), although the increase in B/Ca for a given pH change was more strongly pronounced at higher $[B_T]$. In the experiments where $[B_T]$ was varied at a constant pH of 8.25, B/Ca was positively correlated with $[B_T]$ (Fig. 5C). But notably, the increasing trend gradually leveled out at higher $[B_T]$. By and large, a similar asymptotic profile was found for the covariance between B/Ca and [DIC] (Fig. 5D). Raising [DIC] by 50% from the control caused a substantial increase in B/Ca by 71.8 μmol/mol on average. However, in response to an additional 50% increase in [DIC], B/Ca only increased by 20.0 μmol/mol on average. In case of a 25% reduction in [DIC] from the control, B/Ca were largely invariant from the control. A robust positive correlation was found for B/Ca and $[Ca^{2+}]$ (Fig. 5E). For the joint $[Ca^{2+}]$–pH variation experiments, relatively constant R was maintained at two different $[Ca^{2+}]$ and pH combinations at a fixed saturation. In the first set, $[Ca^{2+}]$ and pH was set at 6796 μmol/kg and 8.00, respectively ($SI_{Calcite} = 0.55$, $\log_{10}R = -5.94 \pm 0.03$). In the second set, pH was raised to 8.37 while $[Ca^{2+}]$ was reduced to 2978 μmol/kg ($SI_{Calcite} = 0.55$, $\log_{10}R = -6.02 \pm 0.02$, see Fig. 5E and F). The average B/Ca for these experiments was 14.6 ± 3.1 and 19.4 ± 5.6 μmol/mol, respectively. When these parameters were separately manipulated, B/Ca co-varied with $[Ca^{2+}]$ and pH (Fig. 5A and E). However, the effects on B/Ca vanished when $[Ca^{2+}]$ and pH were jointly varied (Fig. 5A, E and F).

5. DISCUSSION

5.1. Comparison with previous inorganic experiments

We observed an increase in B contents in calcite with $[B_T]$, which is consistent with previous experiments (Kitano et al., 1978; Hemming et al., 1995; Hobbs and Reardon, 1999, see Fig. 6A). In Kitano et al. (1978), calcite precipitation was induced by CO_2 degassing from B-bearing fluids. Hemming et al. (1995) synthesized calcite using a free-drift technique where saturation was gradually raised

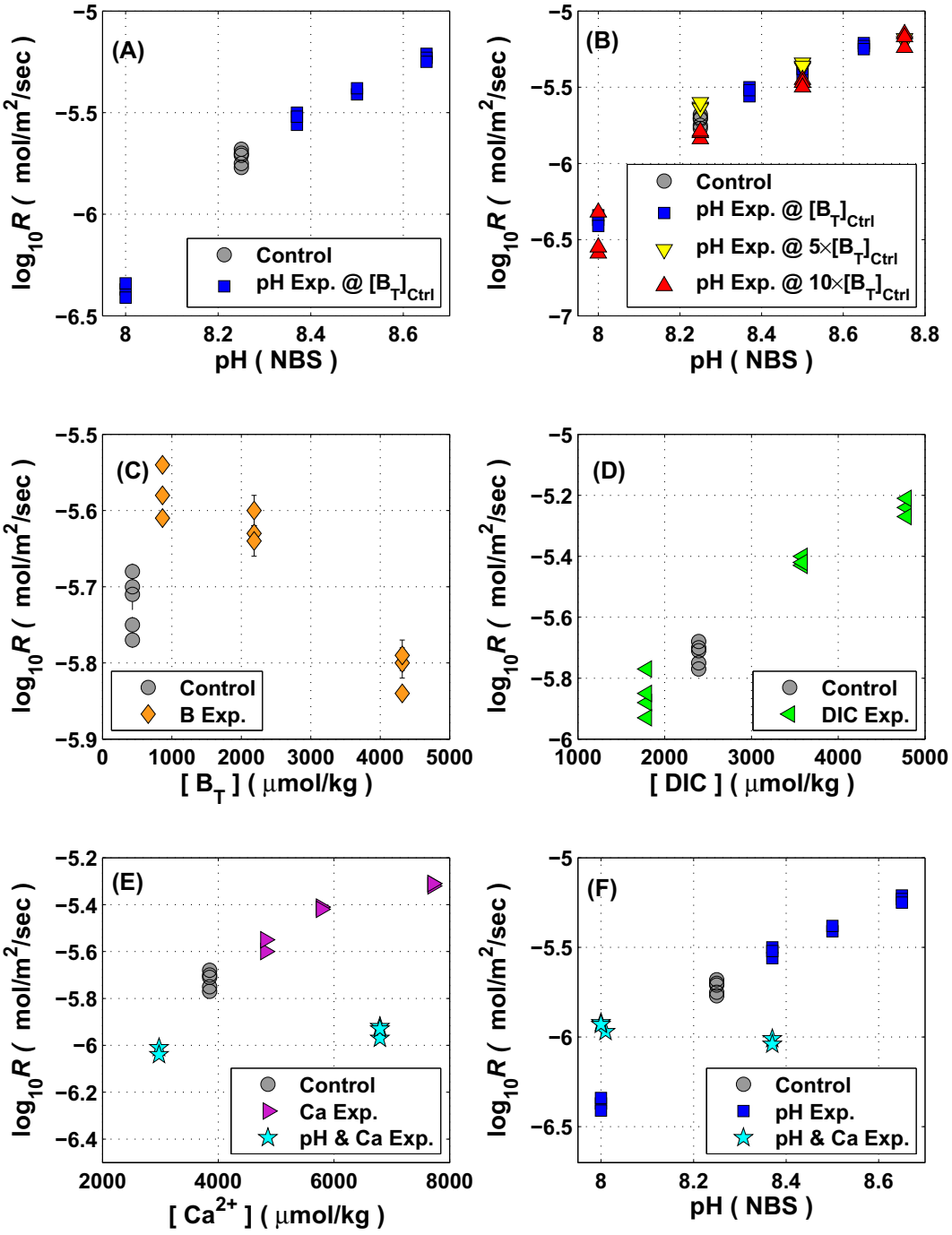

Fig. 4. Changes in calcite precipitation rate R (in mol/m^2/s) due to chemical manipulations tested in this study (see Table 1 for a summary of the chemical manipulations). The error-bars represent 2σ standard deviation (see text for detail). The error-bars were typically much smaller than the size of data symbols.

by diffusion of CO_2 and NH_3 from decomposition of $(NH_4)_2CO_3$ in a closed chamber. Hobbs and Reardon (1999) studied B uptake during the transformation of metastable vaterite and aragonite precursors into calcite. Irrespective of the experimental methods, these studies demonstrated that B contents in calcite depend on $[B_T]$ in solution. Interestingly however, the increasing B/Ca trend gradually tapered off at higher $[B_T]$ ($>\sim$2500 μmol/kg) in our study. Such asymptotic response is unlike the monotonic increase shown by Hemming et al. (1995) and Hobbs and Reardon (1999). Importantly, we also observed a reduction in $\log_{10}R$ from -5.58 ± 0.04 to -5.81 ± 0.03 corresponding to an increase in $[B_T]$ from 864 to 4317 μmol/kg (compare Panel C in Figs. 4 and 5). As we will explain in the following sections, the reduction in R at higher $[B_T]$ appears to be a critical factor for the asymp-

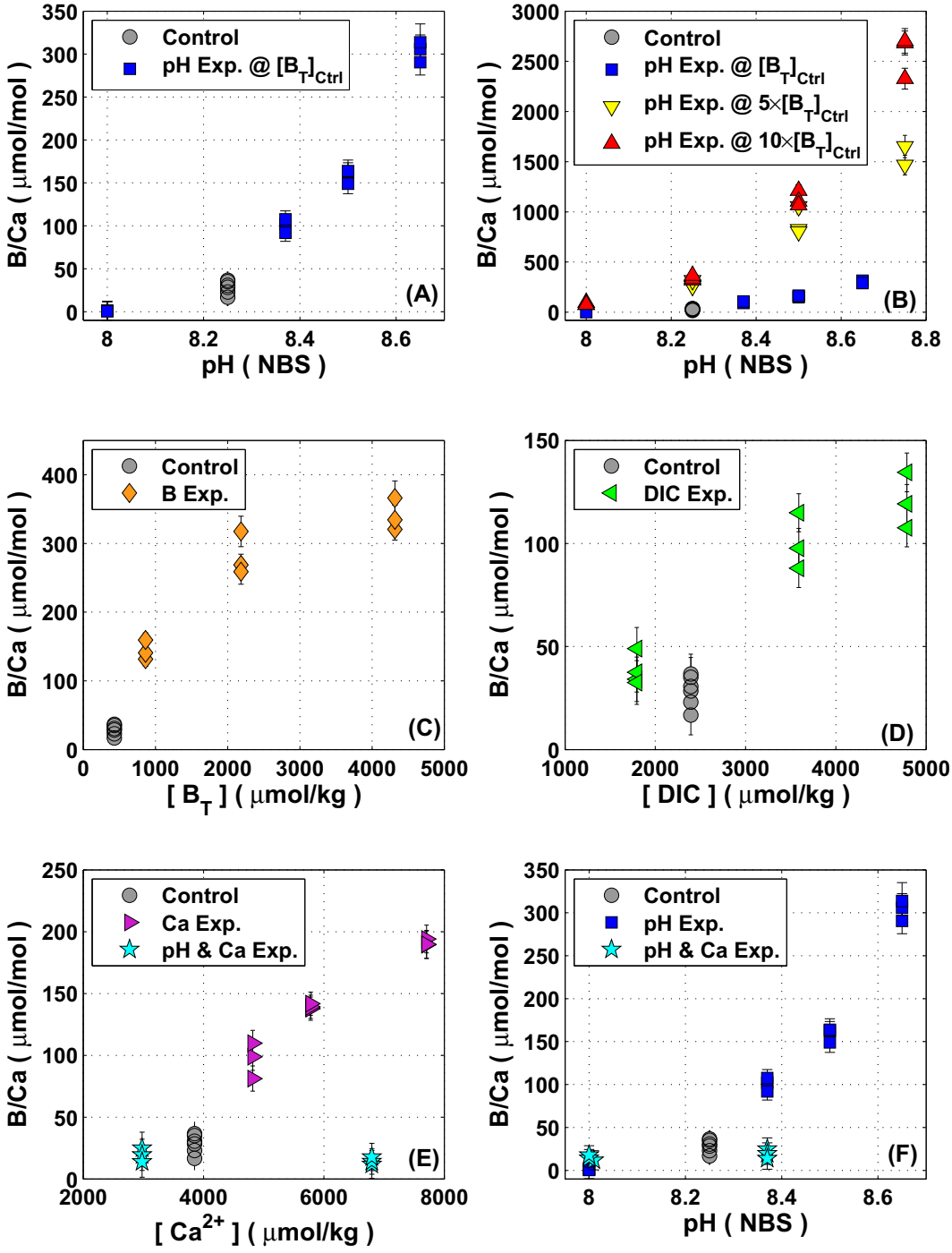

Fig. 5. The effect of chemical manipulations on B contents in calcite overgrowth (see Table 1 for a summary of the chemical manipulations). The error-bars represent 2σ standard deviation for the B/Ca values (see text for detail).

totic behavior of B/Ca in our dataset. However, since precipitation rates were not reported in the earlier studies, it is difficult to comment on whether R similarly played a critical role in the previously observed monotonic increase in B/Ca with $[B_T]$ in Hemming et al. (1995) and Hobbs and Reardon (1999).

Fig. 6B compares the results of our pH variation experiments to those of Sanyal et al. (2000) and He et al. (2013). The figure shows that B/Ca increases with pH in all experimental studies. In our case, the pH experiments were performed at three different $[B_T]$ ($[B_T]_{Ctrl} = 432$, $5\times[B_T]_{Ctrl} = 2184$, and $10\times[B_T]_{Ctrl} = 4317$ μmol/kg). In Sanyal et al. (2000) and He et al. (2013), $[B_T]$ was set at ~6846 and ~4160 μmol/kg, respectively, which are roughly 16.5 and 10 times higher than the typical $[B_T]$ in seawater (~416 μmol/kg; Dickson et al., 2007). Note that one set

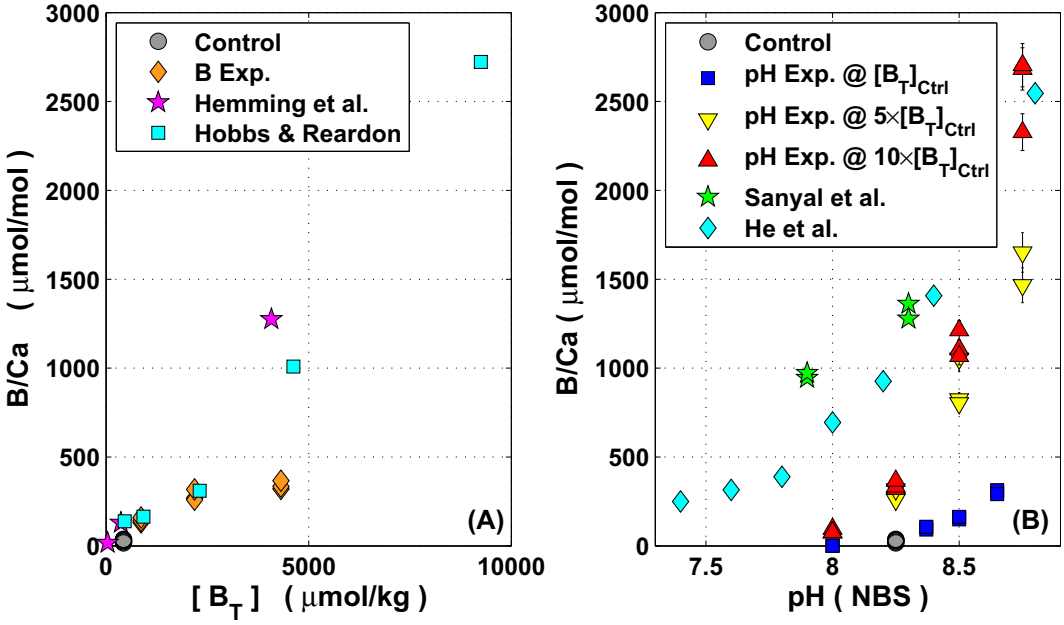

Fig. 6. Comparison of our experimental results with previous inorganic studies. (Panel A) $[B_T]$ variation experiments. The results from Hemming et al. (1995) and Hobbs and Reardon (1999) generally show a monotonic increase in B/Ca with $[B_T]$, whereas our results rather show an asymptotic increase. The pH was maintained at 8.25 in our $[B_T]$ variation experiments, at 8.0 in Hemming et al. (1995) and between 9.0 and 9.1 in Hobbs and Reardon (1999). (Panel B) pH variation experiments. The results compiled here demonstrate a clear pH dependence of B/Ca. Our experiments at $10\times[B_T]_{Ctrl}$ and those by He et al. (2013) were performed at nearly identical $[B_T]$, however, the latter study documented generally higher B/Ca values that are more comparable to Sanyal et al. (2000) presumably due to the difference in $[Ca^{2+}]$. The experimental conditions for the compiled studies are as follows: $[B_T] = \sim 6846$ μmol/kg and $[Ca^{2+}] = \sim 10.3$ mmol/kg (Sanyal et al., 2000); $[B_T] = \sim 4160$ μmol/kg and $[Ca^{2+}] = \sim 51.5$ mmol/kg (He et al., 2013); and $[B_T] = 432$, 2184 and 4317 μmol/kg and $[Ca_{2+}] = \sim 3.9$ mmol/kg (this study).

of our experiments were performed at $[B_T]$ relatively comparable to He et al. (2013) ($[B_T] = 4317$ μmol/kg versus ~4160 μmol/kg). However, their B/Ca values are markedly higher than our data at given pH levels (except for at pH 8.75), and more comparable to Sanyal et al. (2000), despite a major difference in $[B_T]$. This is inconsistent with the dependence of B/Ca on $[B_T]$ (Fig. 6A). The discrepancy can be explained by the positive correlation between B/Ca and $[Ca^{2+}]$ (Fig. 5E, also see below). In our case and Sanyal et al. (2000), calcite precipitation was mediated by the seeds. Because He et al. (2013) did not utilize seeds in their experiments, they were presumably forced to elevate $[Ca^{2+}]$ to overcome the kinetic barrier for the calcite nucleation by raising $SI_{Calcite}$. In their case, $[Ca^{2+}]$ was 51.4 mmol/kg (~5× the typical seawater $[Ca^{2+}]$ of ~10.3 mmol/kg; Dickson et al., 2007), which is significantly higher than $[Ca^{2+}]$ used in our experiments and Sanyal et al. (2000) (~3.9 and ~10.3 mmol/kg, respectively).

5.2. Influence of $[Ca^{2+}]$ on B/Ca

Intuitively, one may expect a decrease in B/Ca in response to an increase in fluid $[Ca^{2+}]$ because the fluid B/Ca ratio decreases (all other parameters held constant). In contrast, we observed a clear increase in B/Ca with $[Ca^{2+}]$ (Fig. 5E). It has been cautioned that the B/Ca proxy may be prone to significant uncertainty due to secular changes in seawater $[B_T]$, particularly when applied to deep times (Lemarchand et al., 2002; Simon et al., 2006). But the observed $[Ca^{2+}]$ effect suggests secular changes in seawater $[Ca^{2+}]$ (Horita et al., 2002; Tyrrell and Zeebe, 2004) may represent an additional complication to interpret B/Ca records, if the effect is also applicable to foraminifera.

Changing $[Ca^{2+}]$ in the parent fluids had a negligible impact on the relative distribution of the dissolved B and DIC species, yet, it substantially altered $SI_{Calcite}$ and R. The observed increase in B/Ca with $[Ca^{2+}]$ can be driven by $[Ca^{2+}]$ change itself, or alternatively it may be related to R rather than $[Ca^{2+}]$. To clarify this issue, we performed a set of experiments where both $[Ca^{2+}]$ and pH were varied at a fixed $SI_{Calcite}$, which resulted in largely invariant B/Ca (Fig. 5E). The total range of $[Ca^{2+}]$ variation in the joint $[Ca^{2+}]$–pH experiments was 3818 μmol/kg, whereas it was 3855 μmol/kg for the simple $[Ca^{2+}]$ variation experiments, which resulted in a ~160 μmol/mol of increase in B/Ca (Fig. 5E). If raising $[Ca^{2+}]$ itself were ultimately responsible for the increase in B/Ca, we would expect to see a notable change in B/Ca for the joint $[Ca^{2+}]$–pH experiments too. But this was not the case. These results imply that the $[Ca^{2+}]$ effect on B/Ca is a manifestation of kinetic effects related to precipitation rate R. It is also important to notice that the pH effect on B/Ca likewise is absent in the joint $[Ca^{2+}]$–pH experiments (Fig. 5F). This strongly suggests that the pH dependence of B/Ca demonstrated here and previously (see Fig. 6B) is in part, and potentially significantly, driven by kinetic effects related to R (see below).

5.3. Kinetic effects on boron incorporation into calcite

Kinetic effects on the incorporation of divalent alkaline earth metals (Mg^{2+}, Sr^{2+}, Ba^{2+}, etc.) into $CaCO_3$ polymorphs have been extensively studied (*e.g.*, Lorens, 1981; Mucci, 1986; Tesoriero and Pankow, 1996; Tang et al., 2008a; Gabitov et al., 2014a). But comparatively less is known about kinetic effects for B incorporation. Hobbs and Reardon (1999) quantified B contents in calcite transformed from initially B-free vaterite and aragonite precursors in B-bearing solutions saturated with respect to those precursors. The calculated calcite saturation state for the vaterite- and aragonite-saturated solutions were 3.2 and 1.5, respectively. Their results depict greater B contents in the calcite transformed from vaterite. Although the rates of calcite formation (or polymorphic transformation) were not explicitly measured, they argued that calcite crystals likely formed more rapidly from vaterite than from aragonite due to the difference in the calcite saturation state for the solutions saturated with respect to those metastable precursors. Hobbs and Reardon (1999) thus attributed kinetic effects as the dominant control for the difference in B contents. Gabitov et al. (2014b) synthesized calcite based on a CO_2 and NH_3 diffusion technique similar to Hemming et al. (1995). They additionally applied sequential injection of rare earth elements over the course of experiments to estimate specific crystal growth rates. Their results reveal a strong covariance between B contents and specific linear growth rates in distinct crystal regions.

It is important to note that all of the chemical manipulations tested here caused changes in $SI_{Calcite}$ and/or R (Fig. 4), which implicitly suggests that the B/Ca variability in our dataset is to some extent controlled by kinetic effects related to R. But other factors must also be involved, as the B/Ca variability in our dataset cannot be comprehensively explained by R alone (Fig. 7). Kinetic effects on the incorporation of certain cations in $CaCO_3$ are typically visualized by plotting the distribution coefficients $K_{Me} = (Me/Ca)_{CaCO_3}/([Me]/[Ca^{2+}])_{Fluid}$ against R, where Me stands for metals such as Sr and Mg. This expression is also denoted frequently as D_{Me} (*e.g.*, Mucci, 1986; Tang et al., 2008a; Gabitov et al., 2014a). Our B/Ca data can be analogously expressed as $K_B = (B/Ca)_{Calcite}/([B_T]/[Ca^{2+}])_{Fluid}$ and plotted against R. This approach also enables us to directly compare our results to Gabitov et al. (2014b) in the same reference frame. Fig. 8 illustrates the consistency between our results and those by Gabitov et al. (2014b) for the overlapping range of R.

Gabitov et al. (2014b) referred to the growth entrapment model (GEM) by Watson (2004) to explain the kinetic enrichment of B at higher linear calcite growth rate (V). GEM posits that the extent of element enrichment and its deviation from the equilibrium depend on the competition between V and the diffusivity of the elements within the outermost regions of the growing crystals. The diffusion acts to eliminate the elements in excess in the surface reactive layers. Thus, higher crystal growth rates would promote element entrapment, whereas less entrapment occurs at slower growth rates. Element diffusivity in the surface reactive layers (D_S) and the degree of element enrichment in the surface reactive layers relative to the crystal interior that is assumed to be in equilibrium (denoted as the surface enrichment factor F) represent two critical parameters of the GEM. The overall composition of the crystal shifts from

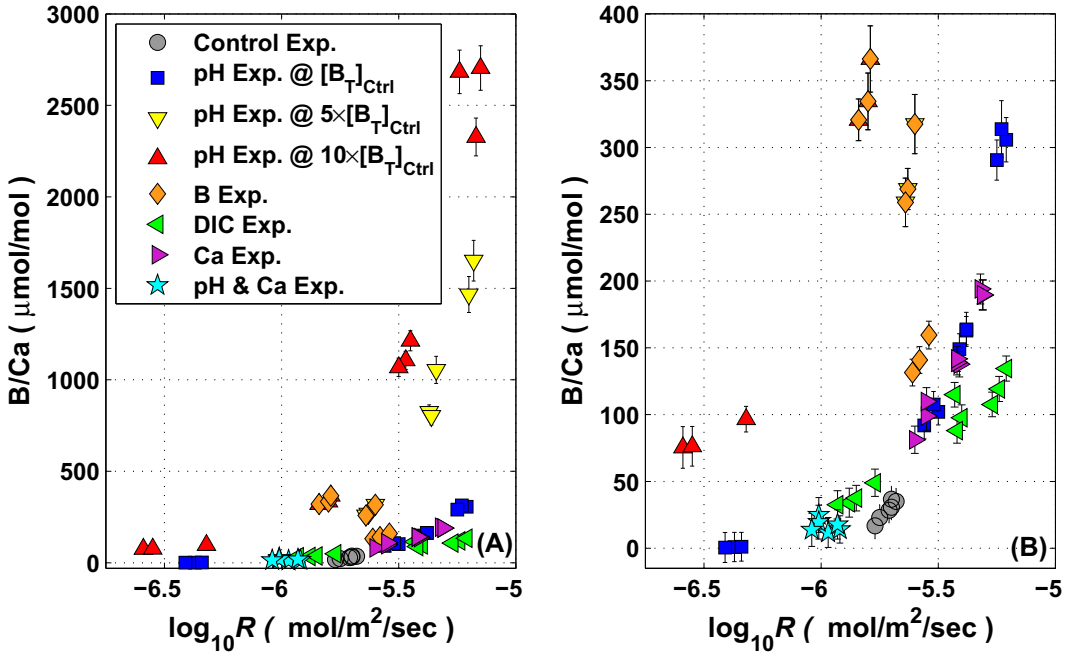

Fig. 7. (Panel A) Relationship between B/Ca and calcite precipitation rate R. The figure shows that B/Ca is not a simple function of R, implying the presence of additional chemical control(s) on B incorporation in calcite. The error-bars are based on the 2σ standard deviations for the $\log_{10} R$ and B/Ca values. The $\log_{10} R$ error-bars were on the order of 0.01 and were masked by the symbols (Panel B) A close-up view of Panel A.

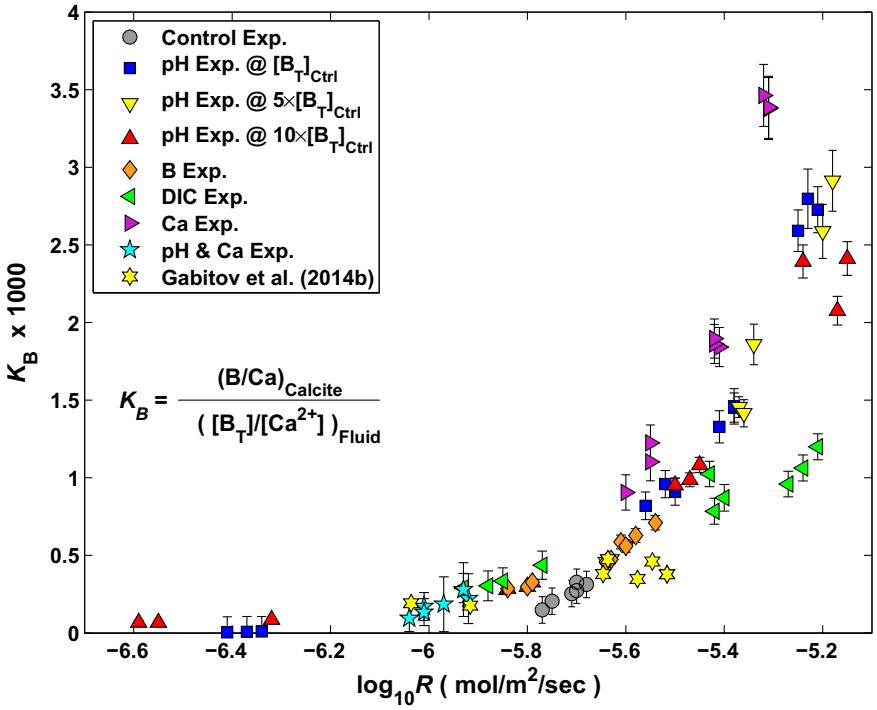

Fig. 8. Comparison of our experimental results with those from Gabitov et al. (2014b). The B/Ca data from both studies are reported here as $K_B = (B/Ca)_{Calcite}/([B_T]/[Ca^{2+}])_{Fluid}$ and plotted against precipitation rate R.

the equilibrium to the enriched signature (dictated by F) with an increase in linear crystal growth rate V. The transition pattern from the equilibrium to the enriched signature as a function of V is typically manifested as a sigmoid curve, and the overall shape of the curvature depends on D_S (see Fig. 4 in Gabitov, 2013). Previous GEM simulations show good agreement with experimentally derived correlations between V and the abundance of certain alkaline earth metals and stable isotopes in synthetic $CaCO_3$ (Watson, 2004; Gaetani and Cohen, 2006; Tang et al., 2008a, 2008b; Gabitov, 2013; Gabitov et al., 2014a). Gabitov et al. (2014b) also found a good agreement between the GEM simulations and the trend of B enrichment with V. Although such a mechanism of surface entrapment is certainly possible, the model-data agreement in Gabitov et al. (2014b) has to be taken with caution because it appears to be partly aided by the optimization of D_S for B in their GEM runs. Despite it being a highly sensitive parameter, D_S is poorly constrained and typically needs to be estimated or optimized somewhat arbitrarily. Moreover, Gabitov et al. (2014b) relied on the experimental results of Hemming et al. (1995) to derive the F value of 28.1 for B. However, it is uncertain if the equilibrium and maximum B entrapment were faithfully reflected by these experimental data.

Kinetically controlled B enrichment could also be explained by the surface kinetic model (SKM) by DePaolo (2011). The SKM considers mineral dissolution as the removal mechanism for the entrapped elements and/or stable isotopes in the surface reactive layers. In a sense, the SKM is similar to the GEM, yet the extent of element/isotope partitioning is viewed as a result of a competition between precipitation rate R and the molecular exchange at the solid–fluid interface through dissolution-reprecipitation cycles. The formulation of the SKM consists of the ratio of the net to gross precipitation rate as well as the element distribution coefficient at the equilibrium (for extremely slow R) and at the kinetic maximum (for extremely rapid R). SKM simulations also showed consistency with R-dependent enrichment of Sr, Mn and ^{16}O and ^{40}Ca (over ^{18}O and ^{44}Ca, respectively) in synthetic calcite (DePaolo, 2011). However, like GEM, the ability of the SKM can be compromised by how the distribution coefficient at the equilibrium and kinetic maximum are defined, which is still largely unknown for B.

Nielsen et al. (2013) proposed a microscopic kinetic model, where the effect of R on the Sr and Mg partitioning in calcite as well as their inhibitory effect on R are simultaneously explained by ionic interactions at active growth kinks. This is an interesting consideration for our $[B_T]$ experiments, for which we observed a general decrease in R and an asymptotic increase in B/Ca with an increase in $[B_T]$ (see Panel C in Fig. 4 and in Fig. 5). Certain dissolved constituents such as Mg^{2+} in solution are known to retard $CaCO_3$ precipitation (Davis et al., 2000; Zeebe and Sanyal, 2002, also see references therein) by blocking the growth kinks and by increasing the mineral solubility via lattice distortion. For anions, Mucci (1986) found that precipitation rate of magnesian calcite decreases with an increase in $[PO_4^{3-}]$. Furthermore, the PO_4^{3-} inhibitory effect was more evident at lower mineral saturation. Mucci (1986) postulated that the outermost regions of the crystals were

exposed to the fluid for a longer duration at lower saturation before they were buried under newly forming layers. This promoted more interactions with PO_4^{3-} at the growth kinks and steps. The decreasing trend in R with $[B_T]$ revealed in this study may also indicate the inhibitory effect by B at growth kinks and steps. Ruiz-Agudo et al. (2012) observed that presence of B leads to roughening and distortion of the growing steps on the $\{10\bar{1}4\}$ calcite crystal surface, which further supports an inhibitory effect by B. The asymptotic increase in B/Ca with $[B_T]$ (Fig. 5C) may hence reflect kinetic suppression, where lowering of R from the inhibitory effect by B led to less B incorporation (*e.g.*, Watson, 2004; DePaolo, 2011).

5.4. Mode of boron incorporation

The plot of $K_B = (B/Ca)_{Calcite}/([B_T]/[Ca^{2+}])_{Fluid}$ versus $\log_{10}R$ shows notable scatter in the domain where $\log_{10}R > -5.5$ or so (Fig. 8). This implies that data parameterization as K_B does not fully capture the chemical controls on B/Ca. A key issue is that, unlike cations (Sr^{2+}, Mg^{2+}, etc.), most likely B is not replacing Ca position in $CaCO_3$. Consequently, rather than Ca^{2+}, DIC species either as specific ions (Hemming and Hanson, 1992) or as a whole (Allen et al., 2011, 2012) should be considered for B incorporation in $CaCO_3$. Hemming and Hanson (1992) proposed the fluid-calcite B distribution coefficient K_D (Eq. (3)). But because the applicability of K_D is still questionable (*e.g.*, Allen and Hönisch, 2012), we also considered a number of "apparent" B partition coefficients:

$$\lambda_{DIC}^{B(OH)4} = \frac{(B/Ca)_{CaCO_3}}{\left(\frac{[B(OH)_4^-]}{[HCO_3^- + CO_3^{2-}]}\right)_{Fluid}} \quad (8)$$

$$\lambda_{HCO3}^{BT} = \frac{(B/Ca)_{CaCO_3}}{\left(\frac{[B_T]}{[HCO_3^-]}\right)_{Fluid}} \quad (9)$$

$$\lambda_{DIC}^{BT} = \frac{(B/Ca)_{CaCO_3}}{\left(\frac{[B_T]}{[HCO_3^- + CO_3^{2-}]}\right)_{Fluid}} \quad (10)$$

Note that these apparent B partition coefficients are different from the traditional distribution coefficients and do not represent stoichiometrically-balanced elementary reactions (such as K_D, see Eqs. (2) and (3)). As the measure of the effectiveness of these expressions (Eqs. (3) and (8)–(10)) in explaining the B/Ca variability, we employed r^2 values obtained from the least squares fitting of the dataset to a basic exponential function $y = A \cdot e^{m \cdot \log_{10}R}$, where A and m are coefficients optimized for the best fit to the data (the values of A and m are listed in Table S2 in Supplementary materials). Note that similar exponential dependence of K_{Me} for Mg and Sr on $\log R$ have been experimentally demonstrated (*e.g.*, Mucci, 1986; Tang et al., 2008a).

In Fig. 9A, the traditional B distribution coefficient K_D (Hemming and Hanson, 1992: Eq. (3)) is plotted against $\log_{10}R$. But this clearly fails to resolve the data scatter for $\log_{10}R > -5.5$ (Fig. 9). The use of $\lambda_{DIC}^{B(OH)_4}$ (Eq. (8)) similarly fails to reduce the scatter at $\log_{10}R > -5.5$ (Fig. 9B). The r^2 values for K_D and $\lambda_{DIC}^{B(OH)_4}$ are 0.79 and 0.81, respectively. But a more convergent picture emerges if the B/Ca data are expressed as $\lambda_{HCO_3}^{BT}$ ($r^2 = 0.88$, see Eq. (9) and Fig. 9C) or as λ_{DIC}^{BT} ($r^2 = 0.89$, see Eq. (10) and Fig. 9D). In our experiments, HCO_3^- was the most abundant DIC species in the parent fluids, whereas CO_3^{2-} typically accounted for 10% of the DIC pool at most. Thus, parameterization using $[HCO_3^- + CO_3^{2-}]$ as opposed to $[HCO_3^-]$ exerts minor control on the overall data distribution (compare Panels A vs B and C vs D in Fig. 9). However, the use of $[HCO_3^- + CO_3^{2-}]$ may be theoretically more appropriate because $CaCO_3$ can be derived from both HCO_3^- and CO_3^{2-} (Wolthers et al., 2012). This requires further testing at higher pH levels, where CO_3^{2-} becomes more abundant. Also note that the $[HCO_3^- + CO_3^{2-}]$ term in $\lambda_{DIC}^{B(OH)_4}$ and λ_{DIC}^{BT} can be simplified as [DIC] in our experimental conditions as well as in most of the oceanic environments (Zeebe and Wolf-Gladrow, 2001) and certainly in the calcification microenvironment of marine organisms (Rink et al., 1998; Al-Horani et al., 2003; Rollion-Bard et al., 2003; Bentov et al., 2009; de Nooijer et al., 2009). In summary, this assessment corroborates that the B/Ca variability caused by a suite of chemical manipulations tested here can be explained by only R and the $[B_T]/[DIC]$ ratio of the parent fluids. Involvement of the latter parameter can be considered as indirect evidence for B incorporation not just via $B(OH)_4^-$ (Hemming and Hanson, 1992) but also via $B(OH)_3$.

The mathematical expression for the exponential curve shown in Fig. 9D is:

$$\lambda_{DIC}^{BT} = A \cdot e^{m \cdot \log_{10}R} \quad (11)$$

where $A = 511{,}112$ and $m = 3.76$ ($r^2 = 0.89$, see Table S2). From the definition of the apparent partition coefficient λ_{DIC}^{BT} (Eq. (10)) and assuming $[HCO_3^- + CO_3^{2-}] \approx [DIC]$, this expression can be rearranged to:

$$(B/Ca)_{Calcite} = \left(\frac{[B_T]}{[DIC]}\right)_{Fluid} \cdot A \cdot R^{m \cdot b} \quad (12)$$

where b ($=1/\log_e 10 \approx 0.43$) is a conversion factor for rescaling $\log_{10}R$ into $\log_e R$ to derive the equation. This B incorporation model reiterates that B/Ca values are controlled by the fluid $[B_T]/[DIC]$ ratio and precipitation rate R. It is important to note that the $[B_T]/[DIC]$ ratio is constant when varying pH, for instance. However, R varies with pH due to the changes in $[CO_3^{2-}]$ and the degree of calcite saturation. The model proposed here therefore implies that the dependence of B/Ca on pH documented by Sanyal et al. (2000) and He et al. (2013) (Fig. 6B) was not controlled by the consequential changes in $[B(OH)_4^-]$, but by the precipitation rate R, which changes with pH (unfortunately R values were not reported in their publication). This view is supported by our results from pH variation, $[Ca^{2+}]$ variation and joint pH–$[Ca^{2+}]$ variation experiments (Fig. 5E and F). In our joint pH–$[Ca^{2+}]$ experiments, B/Ca remains essentially constant despite a large increase in pH and $[B(OH)_4^-]$ (Fig. 5F).

This B incorporation model requires further validation with additional inorganic experiments under various conditions. For instance, it is unclear if the proposed B incorporation model holds for the entire R range covered in

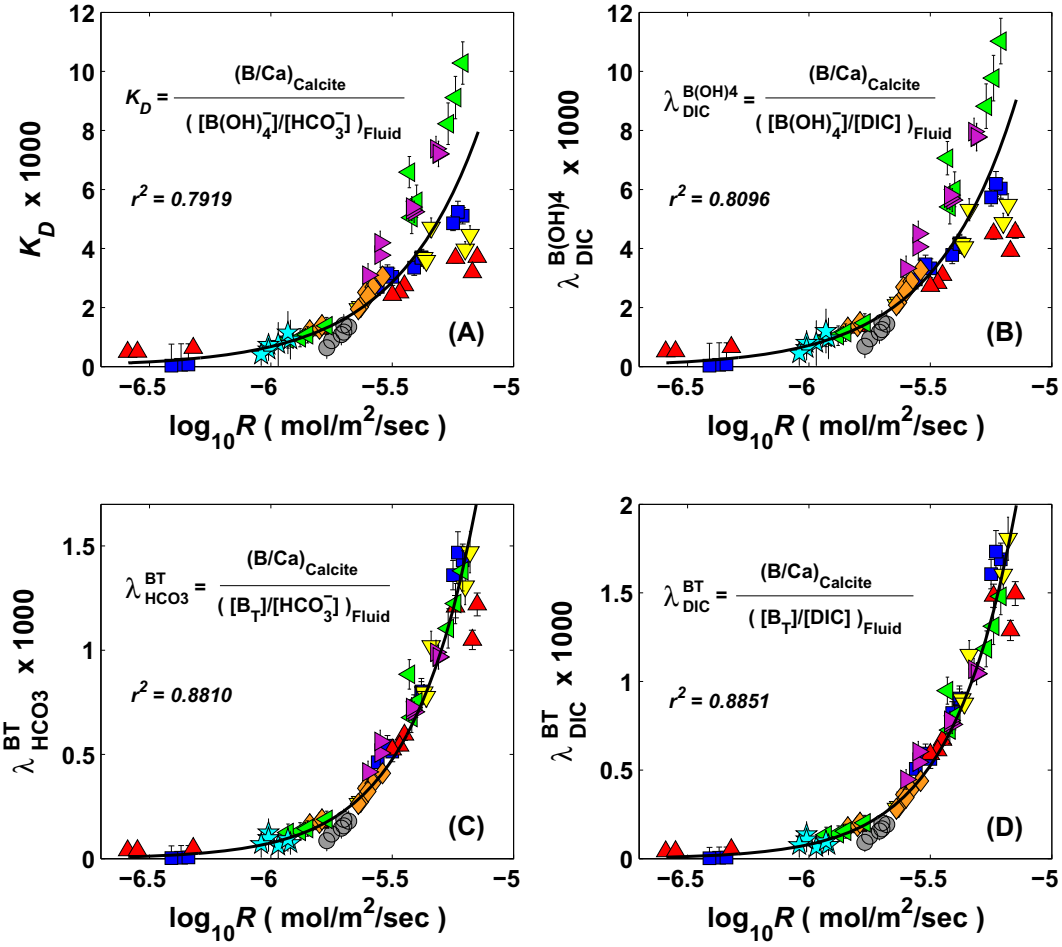

Fig. 9. Comparative assessment of four different B partition coefficients: K_D (Eq. (3), Panel A), $\lambda^{B(OH)_4}_{DIC}$ (Eq. (8), Panel B), $\lambda^{BT}_{HCO_3}$ (Eq. (9), Panel C) and λ^{BT}_{DIC} (Eq. (10), Panel D). The black curve in each panel represents the best-fit exponential function ($y = A \cdot e^{m \cdot x}$, where A and m are coefficients) based on least squares approach. See Table S1 in Supplemental materials for the numerical values for A and m. Note that data parameterization with $[B_T]$ instead of $[B(OH)_4^-]$ substantially reduced the data scatter, especially for $\log_{10} R > -5.5$ (Panels A and B versus Panels C and D). For data legend, refer to Figs. 4–8.

this study. The impact of the use of $[B_T]$ as opposed to $[B(OH)_4^-]$ (in other words, $\lambda^{BT}_{HCO_3}$ and λ^{BT}_{DIC} versus K_D and $\lambda^{B(OH)_4}_{DIC}$) is most evident for $\log_{10} R > -5.5$ or so (Fig. 9). In contrast, for $\log_{10} R < -6$ or so, it is difficult to assess whether the parameterization using $[B_T]$ or $[B(OH)_4^-]$ provides a better fit due to relatively limited data availability (Fig. S6). It is possible that the exponential relationship between λ^{BT}_{DIC} and $\log_{10} R$ holds over the entire R range covered in this study. This view suggests that the B incorporation into calcite via $B(OH)_4^-$ as well as $B(OH)_3$ occurs for both rapid and slow precipitation. Alternatively, it is likewise possible that K_D rather than λ^{BT}_{DIC} is more effective in explaining the B/Ca variability for relatively slow precipitation ($\log_{10} R < -6$ or so). It follows that there is a potential threshold in R, below which the primary pathway of B incorporation is via tetrahedrally-coordinated $B(OH)_4^-$ as originally proposed by Hemming and Hanson (1992). Conversely, above the threshold, incorporation of trigonally-coordinated $B(OH)_3$ is kinetically enhanced. More slow precipitation experiments are needed to clarify this issue. Slow precipitation experiments are also crucial to define the extent of B incorporation at thermodynamic equilibrium, for which kinetic effects need to be eliminated. With the current dataset it is unclear if the equilibrium partitioning was successfully reached in this study.

Theoretical work of Tossell (2006) provides some support for $B(OH)_3$ incorporation into calcite. He proposed that B incorporation into $CaCO_3$ follows three stages; (1) initial adsorption of dissolved B species onto $CaCO_3$ surfaces, (2) "chemo-sorption" via $B(OH)_2CO_3^-$ isomers and (3) breakdown or coordination change of the isomers to the structurally simpler form of trigonal BO_3 and tetrahedral BO_4 (see Fig. 9 in Klochko et al., 2009 for illustration). Although verification of this model requires experimental evidence for the existence of the $B(OH)_2CO_3^-$ isomers, he proposed that the isomers can be derived from both $B(OH)_3$ and $B(OH)_4^-$:

$$B(OH)_3 + HCO_3^- \rightarrow B(OH)_2CO_3^- + H_2O \quad (13)$$

$$B(OH)_4^- + HCO_3^- \rightarrow B(OH)_2CO_3^- + H_2O + OH^- \quad (14)$$

His calculations show that the free energy changes for these reactions are only marginally different, meaning that both pathways are almost equally thermodynamically feasible. Both $B(OH)_3$ and $B(OH)_4^-$ is found to be adsorbed onto the reactive surfaces of various clay minerals and metal hydroxides (Su and Suarez, 1995), thus it seems reasonable to assume the same happens for $CaCO_3$ surfaces. But there can be a critical difference on how strongly $B(OH)_3$ and $B(OH)_4^-$ are adsorbed onto the $CaCO_3$ surfaces. Hemming and Hanson (1992) argued that negatively charged $B(OH)_4^-$ should be adsorbed more readily than neutral $B(OH)_3$.

Supposedly both $B(OH)_3$ and $B(OH)_4^-$ come into contact with calcite surfaces, however, $B(OH)_4^-$ may be adsorbed more firmly due to its charge. If so, there should be a greater chance for $B(OH)_3$ to be detached from the surfaces before fully engaging into the chemo-sorption phase upon slow precipitation. But when calcite is forming rapidly, the surface reactive layers are quickly isolated from the surrounding fluid as they are constantly buried under newly forming layers. In this case, adsorbed $B(OH)_3$ should have a greater chance of being trapped and incorporated before detachment. This should increase the contribution of $B(OH)_3$ relative to $B(OH)_4^-$ for the chemo-sorption and ultimate incorporation. Also note that elimination of such enriched signature becomes progressively ineffective as R increases (Watson, 2004; DePaolo, 2011: see Section 5.3). This explanation based on precipitation kinetics nicely fits with the observed agreement between the experimental data and the proposed B incorporation model (Eq. (12)), which is particularly robust for higher R values (Fig. 9D).

6. CONCLUSIONS AND IMPLICATIONS

In the majority of experiments performed here, we observed kinetic effects on B incorporation into synthetic calcite. In previous efforts to calibrate foraminiferal B/Ca against certain physicochemical parameters based on core-top data or culture experiments, kinetic effects have not been adequately considered. It is highly recommended to determine foraminiferal calcification rates using effective tracers such as ^{14}C or ^{48}Ca (*e.g.*, Lea et al., 1995) in future culture-based calibration studies.

Most of the B/Ca variability due to different chemical manipulations performed here (Table 1) appears to be explained by calcite precipitation rate R and the $[B_T]/[DIC]$ ratio in the parent fluids. This was particularly the case for $\log_{10}R > -5.75$ or so (Fig. 9D), suggesting the possibility of kinetically controlled enhancement of $B(OH)_3$ incorporation on top of $B(OH)_4^-$ in relatively fast forming $CaCO_3$. In contrast, it is difficult to address the validity of λ_{DIC}^{BT} (and/or K_D) for slower precipitation with confidence due to the shortage of reliable data. Additional slow precipitation experiments are required to resolve this issue. The slow precipitation experiments would also be crucial to better constrain the extent of equilibrium B incorporation. Moreover, all of the experiments presented here were performed at 25 °C, yet temperature variability may impose additional controls on B/Ca in $CaCO_3$. This subject is of debate for the calibrations of planktonic foraminiferal B/Ca (*e.g.*, Allen et al., 2011, 2012; Allen and Hönisch, 2012), which needs to be experimentally evaluated in the future.

It is unclear if foraminifera B/Ca is directly influenced by kinetically controlled $B(OH)_3$ incorporation proposed here. Due to large uncertainties in the surface area estimates of structurally-complex shell surfaces, foraminiferal calcification rates are rarely normalized to the shell surface area. However, some estimates suggest surface area normalized calcification rates of about 1000–4000 μmol/m^2/h in planktonic and benthic foraminifers (Carpenter and Lohmann, 1992; Lea et al., 1995), which translates to $\log_{10}R$ of −6.56 to −5.95 in the unit of mol/m^2/s. This is well below the $\log_{10}R$ range where our experimental data most dominantly indicated the possibility of $B(OH)_3$ incorporation into calcite (Figs. 9 and S6). One caveat is that these foraminiferal calcification rates were derived from culture experiments in which only the light availability (irradiance level) was varied. On the contrary, pH and [DIC] variations were applied in previous culture experiments for planktonic foraminiferal B/Ca (Sanyal et al., 1996; Allen et al., 2011, 2012). Possibility of much higher calcification rates and $B(OH)_3$ contribution for B incorporation in response to such chemical manipulations cannot be ruled out.

Finally, the outcome of this study also has critical implications on the theoretical framework of the $\delta^{11}B$ paleo-pH proxy. Although exclusive incorporation of $B(OH)_4^-$ into $CaCO_3$ is the first order assumption (Hemming and Hanson, 1992), the $\delta^{11}B$ values of biogenic carbonates produced in pH-controlled culture experiments were found to be enriched in ^{11}B relative to the expected $\delta^{11}B$ values of $B(OH)_4^-$ (see Fig. 1C). This has been explained in terms of pH regulation within the calcification microenvironment (Hönisch et al., 2003; Zeebe et al., 2003; Rollion-Bard and Erz, 2010). However, synthetic calcites produced by Sanyal et al. (2000) also show similar positive $\delta^{11}B$ offsets relative to $B(OH)_4^-$ (Fig. 1C). Klochko et al. (2009) consequently argued that the positive offsets in the $\delta^{11}B$ values of both biogenic and synthetic $CaCO_3$ can be attributed to partial incorporation of $B(OH)_3$. Importantly, this ^{11}B enrichment in synthetic and biogenic $CaCO_3$ relative to $B(OH)_4^-$ diminishes at higher pH, which is not consistent with our experimental outcome. Our results support the possibility of greater $B(OH)_3$ incorporation into calcite at higher precipitation rates (Fig. 9D). Because $SI_{Calcite}$ and R increases with pH, one would expect greater $B(OH)_3$ contribution at higher pH. In this scenario, the positive offset in Fig. 1C would be more strongly pronounced at higher pH. However, this will be the case *only if* the original isotopic compositions of $B(OH)_4^-$ and $B(OH)_3$ are faithfully preserved in $CaCO_3$. Exchange of B isotopes between $B(OH)_3$ and $B(OH)_4^-$ is extremely rapid. For example, isotopic equilibration between these two species comes to completion within ~125 micro-seconds (Zeebe et al., 2001). Thus changes in the $\delta^{11}B$ values of dissolved B species during the adsorption onto and incorporation into $CaCO_3$ is possible due to rapid isotope exchange. Another open question

is the possibility of preferential incorporation of light isotopes upon rapid precipitation. Previous inorganic studies demonstrated that the magnitude of calcite-fluid stable Ca and O isotope fractionation decreases with R due to preferential uptake of ^{40}Ca and ^{16}O over ^{44}Ca and ^{18}O upon rapid precipitation (Tang et al., 2008b; Dietzel et al., 2009; Gabitov et al., 2012; Watkins et al., 2014), which is in agreement with theoretical calculations using the surface kinetic model (DePaolo, 2011). If the uptake of $^{10}B(OH)_3$ is similarly favored over $^{11}B(OH)_3$ at higher precipitation rates, kinetic enhancement of $B(OH)_3$ incorporation implied by our experimental data may be compatible with the observed decrease in the positive $\delta^{11}B$ offset between biogenic/synthetic calcites and $B(OH)_4^-$ with pH (Fig. 1C). Measurement of $\delta^{11}B$ values of some of the samples produced in this study will hopefully help to resolve the conundrum in the future.

ACKNOWLEDGEMENTS

This research was supported by NSF grant OCE–1333357 to R.E.Z. Michael Guidry and Roy Tom are credited for their support on designing and crafting of the reaction chamber. We are grateful to Rob Franks and Dyke Andreasen for their analytical support in the laboratory. We thank Gavin Foster and two anonymous reviewers for constructive comments, which improved this manuscript. We also thank Robert Byrne for editorial handling. J.U. acknowledges the KAYO-RECOV Project. This is SOEST Publication #9239.

APPENDIX A. SUPPLEMENTARY DATA

Supplementary data associated with this article can be found, in the online version, at http://dx.doi.org/10.1016/j.gca.2014.11.022.

REFERENCES

Al-Ammar A., Gupta R. K. and Barnes R. M. (1999) Elimination of boron memory effect in inductively coupled plasma-mass spectrometry by addition of ammonia. *Spectrochim. Acta, Part B* **54**, 1077–1084.

Al-Horani F. A., Al-Moghrabi S. M. and de Beer D. (2003) Microsensor study of photosynthesis and calcification in the scleractinian coral, *Galaxea fascicularis*: active internal carbon cycle. *J. Exp. Mar. Biol. Ecol.* **288**, 1–15.

Allen K. A. and Hönisch B. (2012) The planktic foraminiferal B/Ca proxy for seawater carbonate chemistry: a critical evaluation. *Earth Planet. Sci. Lett.* **345–348**, 203–211.

Allen K. A., Hönisch B., Eggins S. M., Yu J., Spero H. J. and Elderfield H. (2011) Controls on boron incorporation in cultured tests of the planktic foraminifer *Orbulina universa*. *Earth Planet. Sci. Lett.* **309**, 291–301.

Allen K. A., Hönisch B., Eggins S. M. and Rosenthal Y. (2012) Environmental controls on B/Ca in calcite tests of the tropical planktic foraminifer species *Globigerinoides ruber* and *Globigerinoides sacculifer*. *Earth Planet. Sci. Lett.* **351–352**, 270–280.

Allison N. and Finch A. A.EIMF (2010) $\Delta^{11}B$, Sr, Mg and B in a modern *Porites* coral: the relationship between calcification site pH and skeletal chemistry. *Geochim. Cosmochim. Acta* **74**, 1790–1800.

Barker S., Greaves M. and Elderfield H. (2003) A study of cleaning procedures used for foraminiferal Mg/Ca paleothermometry. *Geochem. Geophys. Geosyst.* **4**, 8407. http://dx.doi.org/10.1029/2003GC000559.

Ball J. W. and Nordstrom D. K. (1991) User's manual for WATEQ4F, with revised thermodynamic data base and test cases for calculating speciation of major, trace, and redox elements in natural waters. U.S. Geological Survey Open-File Report 91-183.

Bartoli G., Hönisch B. and Zeebe R. E. (2011) Atmospheric CO_2 decline during the Pliocene intensification of Northern Hemisphere glaciations. *Paleoceanography* **26**, PA4213. http://dx.doi.org/10.1029/2010PA002055.

Bentov S., Brownlee C. and Erez J. (2009) The role of seawater endocytosis in the biomineralization process in calcareous foraminifera. *Proc. Natl. Acad. Sci.* **106**, 21500–21504.

Brown R. E., Anderson L. D., Thomas E. and Zachos J. C. (2011) A core-top calibration of B/Ca in the benthic foraminifers *Nutallides umbonifera* and *Oridorsalis umbonatus*: a proxy for Cenozoic bottom water carbonate saturation. *Earth Planet. Sci. Lett.* **310**, 360–368.

Carpenter S. J. and Lohmann K. C. (1992) Sr/Mg ratios of modern marine calcite: empirical indicators of ocean chemistry and precipitation rate. *Geochim. Cosmochim. Acta* **56**, 1837–1849.

Davis K. J., Dove P. M. and De Yoreo J. J. (2000) The role of Mg^{2+} as an impurity in calcite growth. *Science* **290**, 1134–1137.

de Nooijer L. J., Toyufuku T. and Kitazato H. (2009) Foraminifera promote calcification by elevating their intracellular pH. *Proc. Natl. Acad. Sci.* **106**, 15374–15378.

DePaolo D. J. (2011) Surface kinetic model for isotopic and trace element fractionation during precipitation of calcite from aqueous solutions. *Geochim. Cosmochim. Acta* **75**, 1039–1056.

Dietzel M., Tang J., Leis A. and Köhler S. J. (2009) Oxygen isotopic fractionation during inorganic calcite precipitation – effects of temperature, precipitation rate and pH. *Chem. Geol.* **268**, 107–115.

Dickson, A.G., Sabine, C.L., Christian, J.R. 2007. Guide to Best Practices for Ocean CO_2 Measurements, PICES Special Publication, 3, 191 pp.

Doss W. and Marchitto T. M. (2013) Glacial deep ocean sequestration of CO_2 driven by the eastern equatorial Pacific biological pump. *Earth Planet. Sci. Lett.* **377–378**, 43–54.

Foster G. L. (2008) Seawater pH, pCO_2 and $[CO_3^{2-}]$ variations in the Caribbean Sea over the last 130 kyr: a boron isotope and B/Ca study of planktic foraminifera. *Earth Planet. Sci. Lett.* **271**, 254–266.

Foster G. L., Pogge von Strandmann P. A. E. and Rae J. W. (2010) Boron and magnesium isotopic composition of seawater. *Geochem. Geophys. Geosyst.* **11**, Q08015. http://dx.doi.org/10.1029/2010GC003201.

Gabitov R. I. (2013) Growth-rate induced disequilibrium of oxygen isotopes in aragonite: an *in situ* study. *Chem. Geol.* **351**, 268–275.

Gabitov R. I., Watson E. B. and Sadekov A. (2012) Oxygen isotope fractionation between calcite and fluid as a function of growth rate and temperature: an in situ study. *Chem. Geol.* **306–307**, 92–102.

Gabitov R. I., Sadekov A. and Leinweber A. (2014a) Crystal growth rate effect on Mg/Ca and Sr/Ca partitioning between calcite and fluid: an in situ approach. *Chem. Geol.* **367**, 70–82.

Gabitov R. I., Rollion-Bard C., Tripati A. and Sadekov A. (2014b) *In situ* study of boron partitioning between calcite and fluid at different crystal growth rates. *Geochim. Cosmochim. Acta* **137**, 81–92.

Gaetani G. A. and Cohen A. L. (2006) Element partitioning during precipitation of aragonite from seawater: a framework for

understanding paleoproxies. *Geochim. Cosmochim. Acta* **70**, 4617–4634.
Green H. G., Blincoe C. and Weeth H. J. (1976) Boron contamination from borosilicate glass. *J. Agric. Food Chem.* **24**, 1245–1246.
He M., Xiao Y., Jin Z., Liu W., Ma Y., Zhang Y. and Luo C. (2013) Quantification of boron incorporation into synthetic calcite under controlled pH and temperature conditions using a differential solubility technique. *Chem. Geol.* **337–338**, 67–74.
Hemming N. G. and Hanson G. N. (1992) Boron isotopic composition and concentration in modern marine carbonates. *Geochim. Cosmochim. Acta* **56**, 537–543.
Hemming N. G., Reeder R. J. and Hanson G. N. (1995) Mineral-fluid partitioning and isotopic fractionation of boron in synthetic calcium carbonate. *Geochim. Cosmochim. Acta* **59**, 371–379.
Henehan M. J., Rae J. W. B., Foster G. L., Erez J., Prentice K. C., Kucera M., Bostock H. C., Martínez-Botí M. A., Milton J. A., Wilson P. A., Marshall B. J. and Elliott T. (2013) Calibration of the boron isotope proxy in the planktonic foraminifera *Globigerinoides ruber* for use in palaeo-CO_2 reconstruction. *Earth Planet. Sci. Lett.* **364**, 111–122.
Hobbs M. Y. and Reardon E. J. (1999) Effect of pH on boron coprecipitation by calcite: further evidence for nonequilibrium partitioning of trace elements. *Geochim. Cosmochim. Acta* **63**, 1013–1021.
Hönisch B. and Hemming N. G. (2005) Surface ocean pH response to variations in pCO_2 through two full glacial cycles. *Earth Planet. Sci. Lett.* **236**, 305–314.
Hönisch B., Bijma J., Russell A. D., Spero H. J., Palmer M. R., Zeebe R. E. and Eisenhauer A. (2003) The influence of symbiont photosynthesis on the boron isotopic composition of foraminifera shells. *Mar. Micropaleont.* **928**, 1–10.
Hönisch B., Hemming N. G., Grottoli A. G., Amat A., Hanson G. N. and Bijma J. (2004) Assessing scleractinian corals as recorders for paleo-pH: empirical calibration and vital effects. *Geochim. Cosmochim. Acta* **68**, 3675–3685.
Hönisch B., Hemming N. G. and Loose B. (2007) Comment on "A critical evaluation of the boron isotope-pH proxy: the accuracy of ancient ocean pH estimates" by M. Pagani, D. Lemarchand, A. Spivack and J. Gaillardet. *Geochim. Cosmochim. Acta* **71**, 1636–1641.
Hönisch B., Hemming G. N., Archer D., Siddall M. and McManus J. F. (2009) Atmospheric carbon dioxide concentration across the Mid-Pleistocene transition. *Science* **324**, 1551–1554.
Horita J., Zimmermann H. and Holland H. D. (2002) Chemical evolution of seawater during the Phanerozoic: implications from the record of marine evaporates. *Geochim. Cosmochim. Acta* **66**, 3733–3756.
Kakihana H., Kotaka M., Satoh S., Nomura M. and Okamoto M. (1977) Fundamental studies on the ion-exchange of boron isotopes. *Bull. Chem. Soc. J.* **50**, 158–163.
Kennett J. P. and Stott L. D. (1991) Abrupt deep-sea warming, paleoceanographic changes and benthic extinctions at the end of the Palaeocene. *Nature* **353**, 225–229.
Kitano Y., Okumura M. and Idogaki M. (1978) Coprecipitation of borate-boron with calcium carbonate. *Geochem. J.* **12**, 183–189.
Klochko K., Kaufman A. J., Yao W., Byrne R. H. and Tossell J. A. (2006) Experimental measurement of boron isotope fractionation in seawater. *Earth Planet. Sci. Lett.* **248**, 276–285.
Klochko K., Cody G. D., Tossell J. A., Dera P. and Kaufman A. J. (2009) Re-evaluating boron speciation in biogenic calcite and aragonite using ^{11}B MAS NMR. *Geochim. Cosmochim. Acta* **73**, 1890–1900.
Lea D. W., Martin P. A., Chan D. A. and Spero H. J. (1995) Calcium uptake and calcification rate in the planktonic foraminifer *Orbulina universa*. *J. Foraminiferal Res.* **25**, 14–23.
Lemarchand D., Gaillardet J., Lewin É. and Allègre C. J. (2002) Boron isotope systematics in large rivers: implications for the marine boron budget and paleo-pH reconstruction over the Cenozoic. *Chem. Geol.* **190**, 123–140.
Liu Y. and Tossell J. A. (2005) Ab initio molecular orbital calculations for boron isotope fractionations on boric acids and borates. *Geochim. Cosmochim. Acta* **69**, 3995–4006.
Lorens R. B. (1981) Sr, Cd, Mn and Co distribution coefficients in calcite as a function of calcite precipitation rate. *Geochim. Cosmochim. Acta* **45**, 553–561.
Lüthi D. et al. (2008) High-resolution carbon dioxide concentration record 650,000–800,000 years before present. *Nature* **453**, 379–382.
Mesmer R. E., Base C. F. and Sweeton F. H. (1972) Acidity measurements at elevated temperatures. VI. Boric acid equilibriums. *Inorg. Chem.* **11**, 537–543.
Mucci A. (1986) Growth kinetics and composition of magnesian calcite overgrowths precipitated from seawater: quantitative influence of orthophosphate ions. *Geochim. Cosmochim. Acta* **50**, 2255–2265.
Ni Y., Foster G. L., Bailey T., Elliott T., Schmidt D. N., Pearson P., Haley B. and Coath C. (2007) A core top assessment of proxies for the ocean carbonate system in surface-dwelling foraminifers. *Paleoceanography* **22**, PA3212. http://dx.doi.org/10.1029/2006PA001337.
Nielsen L. C., De Yoreo J. J. and DePaolo D. J. (2013) General model for calcite growth kinetics in the presence of impurity ions. *Geochim. Cosmochim. Acta* **115**, 100–114.
Parkhurst D. L. and Appelo C. A. J. (1999) User's guide to PHREEQC (version 2) – a computer program for speciation, batch-reaction, one-dimensional transport, and inverse geochemical calculations. U.S. Geological Survey, Water-Resource Investigations Report 99-4259.
Pearson P. N. and Palmer M. R. (2000) Atmospheric carbon dioxide concentrations over the past 60 million years. *Nature* **406**, 695–699.
Penman D. E., Hönisch B., Zeebe R. E., Thomas E. and Zachos J. C. (2014) Rapid and sustained surface ocean acidification during the Paleocene-Eocene Thermal Maximum. *Paleoceanography* **29**, 357–369. http://dx.doi.org/10.1002/2014PA002621.
Plummer L. N. and Busenberg E. (1982) The solubilities of calcite, aragonite and vaterite in CO_2-H_2O solutions between 0 and 90°C, and an evaluation of the aqueous model for the system $CaCO_3$-CO_2-H_2O. *Geochim. Cosmochim. Acta* **46**, 1011–1040.
Rae J. B. R., Foster G. L., Schmidt D. N. and Elliott T. (2011) Boron isotopes and B/Ca in benthic foraminifera: proxies for the deep ocean carbonate system. *Earth Planet. Sci. Lett.* **302**, 403–413.
Raitzsch M., Hathorne E. C., Kuhnert H., Groeneveld J. and Bickert T. (2011) Modern and late Pleistocene B/Ca ratios of the benthic foraminifer *Planulina wuellerstorfi* determined with laser ablation ICP-MS. *Geology* **39**, 1039–1042.
Rickaby R. E. M., Elderfield H., Roberts N., Hillenbrand C.-D. and Mackensen A. (2010) Evidence for elevated alkalinity in the glacial Southern Ocean. *Paleoceanography* **25**, PA1209. http://dx.doi.org/10.1029/2009PA001762.
Rink S., Kühl M., Bijma J. and Spero H. J. (1998) Microsensor studies of photosynthesis and respiration in the symbiotic foraminifer *Orbulina universa*. *Mar. Biol.* **131**, 583–595.
Rohling E. J. et al. (2012) Making sense of paleoclimate sensitivity. *Nature* **491**, 683–691.

Rollion-Bard C. and Erez J. (2010) Intra-shell boron isotope ratios in the symbiont-bearing benthic foraminiferan *Amphistegina lobifera*: implications for $\delta^{11}B$ vital effects and paleo-pH reconstructions. *Geochim. Cosmochim. Acta* **74**, 1530–1536.

Rollion-Bard C., Chaussidon M. and France-Lanord C. (2003) PH control on oxygen isotopic composition of symbiotic corals. *Earth Planet. Sci. Lett.* **215**, 275–288.

Romanek C. S., Grossman E. L. and Morse J. W. (1992) Carbon isotope fractionation in synthetic aragonite and calcite: effects of temperature and precipitation rate. *Geochim. Cosmochim. Acta* **56**, 419–430.

Ruiz-Agudo E., Putnis C. V., Kowacz M., Ortega-Huertas M. and Putnis A. (2012) Boron incorporation into calcite during growth: implications for the use of boron in carbonates as a pH proxy. *Earth Planet. Sci. Lett.* **345–348**, 9–17.

Sanyal A., Hemming N. G., Hanson G. N. and Broecker W. S. (1995) Evidence for a higher pH in the glacial ocean from boron isotopes in foraminifera. *Nature* **373**, 234–236.

Sanyal A., Hemming N. G., Broecker W. S., Lea D. W., Spero H. J. and Hanson G. N. (1996) Oceanic *p*H control on the boron isotopic composition of foraminifera: evidence from culture experiments. *Paleoceanography* **11**, 513–517.

Sanyal A., Hemming N. G., Broecker W. S. and Hanson G. N. (1997) Change in pH in the eastern equatorial Pacific across stage 5–6 boundary based on boron isotopes in foraminifera. *Glob. Biogeochem. Cycles* **11**, 125–133.

Sanyal A., Nugent M., Reeder R. J. and Bijma J. (2000) Seawater pH control on the boron isotopic composition of calcite: evidence from inorganic calcite precipitation experiments. *Geochim. Cosmochim. Acta* **64**, 1551–1555.

Sanyal A., Bijma J., Spero H. and Lea D. W. (2001) Empirical relationship between pH and the boron isotopic composition of *Globigerinoides sacculifer*: implications for the boron isotope paleo-pH proxy. *Paleoceanography* **16**, 515–519.

Sen S., Stebbins J. F., Hemming N. G. and Ghosh B. (1994) Coordination environments of B impurities in calcite and aragonite polymorphs: a ^{11}B MAS NMR study. *Am. Mineral.* **79**, 819–825.

Simon L., Lecuyer C., Marechal C. and Coltice N. (2006) Modeling the geochemical cycle of boron: implications for the long-term $\delta^{11}B$ evolution of seawater and oceanic crust. *Chem. Geol.* **225**, 61–76.

Sinclair D. J., Kinsley L. P. J. and McCulloch M. T. (1998) High resolution analysis of trace elements in corals by laser ablation ICP-MS. *Geochim. Cosmochim. Acta* **62**, 1889–1901.

Spivack A. J., You C.-F. and Smith H. J. (1993) Foraminiferal boron isotope ratio as a proxy for surface ocean pH over the past 21 Myr. *Nature* **363**, 149–151.

Su C. and Suarez D. L. (1995) Coordination of adsorbed boron: a FTIR spectroscopic study. *Environ. Sci. echnol.* **29**, 302–311.

Tang J., Köhler S. J. and Dietzel M. (2008a) Sr^{2+}/Ca^{2+} and $^{44}Ca/^{40}Ca$ fractionation during inorganic calcite formation: I. Sr incorporation. *Geochim. Cosmochim. Acta* **72**, 3718–3732.

Tang J., Dietzel M., Böhm F., Köhler S. J. and Eisenhauer A. (2008b) Sr^{2+}/Ca^{2+} and $^{44}Ca/^{40}Ca$ fractionation during inorganic calcite formation: II. Ca isotopes. *Geochim. Cosmochim. Acta* **72**, 3733–3745.

Tesoriero A. J. and Pankow J. F. (1996) Solid solution partitioning of Sr^{2+}, Ba^{2+}, and Cd^{2+} to calcite. *Geochim. Cosmochim. Acta* **60**, 1053–1063.

Tossell J. A. (2006) Boric acid adsorption on humic acids: *Ab initio* calculation of structures, stabilities, ^{11}B NMR and ^{11}B, ^{10}B isotopic fractionations of surface complexes. *Geochim. Cosmochim. Acta* **70**, 5089–5103.

Tyrrell T. and Zeebe R. E. (2004) History of carbonate ion concentration over the last 100 million years. *Geohim. Cosmochim. Acta* **68**, 3521–3530.

Uchikawa J. and Zeebe R. E. (2010) Examining possible effects of seawater pH decline on foraminiferal stable isotopes during the Paleocene-Eocene Thermal Maximum. *Paleoceanography* **25**, PA2216. http://dx.doi.org/10.1029/2009PA001864.

Vengosh A., Kolodny Y., Starinsky A., Chivas A. R. and McCulloch M. T. (1991) Coprecipitation and isotopic fractionation of boron in modern biogenic carbonates. *Geochim. Cosmochim. Acta* **55**, 2901–2910.

Wara M. W., Delaney M. L., Bullen T. D. and Ravelo A. C. (2003) Possible roles of pH, temperature, and partial dissolution in determining boron concentration and isotopic composition in planktonic foraminifera. *Paleoceanography* **18**(4), 1100. http://dx.doi.org/10.1029/2002PA000797.

Watkins J. M., Hunt J. D., Ryerson F. J. and DePaolo D. J. (2014) The influence of temperature, pH, and growth rate on the δ18O composition of inorganically precipitated calcite. *Earth Planet. Sci. Lett.* **404**, 332–343.

Watson E. B. (2004) A conceptual model for near-surface kinetic controls on the trace-element and stable isotope composition of abiogenic calcite crystals. *Geochim. Cosmochim. Acta* **68**, 1473–1488.

Wolf-Gladrow D. A., Bijma J. and Zeebe R. E. (1999) Model simulation of the carbonate chemistry in the microenvironment of symbiont bearing foraminifera. *Mar. Chem.* **64**, 181–198.

Wolthers M., Nehrke G., Gustafsson J. P. and Cappellen P. V. (2012) Calcite growth kinetics: modeling the effect of solution chemistry. *Geochim. Cosmochim. Acta* **77**, 121–134.

Yu J. and Elderfield H. (2007) Benthic foraminiferal B/Ca ratios reflect deep water carbonate saturation state. *Earth Planet. Sci. Lett.* **258**, 73–86.

Yu J., Elderfield H. and Hönisch B. (2007) B/Ca in planktonic foraminifera as a proxy for surface seawater pH. *Paleoceanography* **22**, PA2202. http://dx.doi.org/10.1029/2006PA001347.

Yu J., Broecker W. S., Elderfield H., Jin Z., McManus J. and Zhang F. (2010) Loss of carbon from the deep sea since the Last Glacial Maximum. *Science* **330**, 1084–1087.

Yu J., Thornalley D. J. R., Rae J. W. B. and McCave N. I. (2013a) Calibration and application of B/Ca, Cd/Ca and $\delta^{11}B$ in *Neogloboquadrina pachyderma* (sinistral) to constrain CO_2 uptake in the subpolar North Atlantic during the last deglaciation. *Paleoceanography* **28**, 237–252. http://dx.doi.org/10.1002/palo.20024.

Yu J., Anderson R. F., Jin Z., Rae J. W. B., Opdyke B. N. and Eggins S. M. (2013b) Responses of the deep ocean carbonate system to carbon reorganization during the Last Glacial-interglacial cycle. *Quat. Sci. Rev.* **76**, 39–52.

Yu J., Anderson R. F., Jin Z., Menviel L., Zhang F., Ryerson F. J. and Rohling E. J. (2014) Deep South Altantic carbonate chemistry and increased interocean deep water exchange during last deglaciation. *Quat. Sci. Rev.* **90**, 80–89.

Zachos J. C., Pagani M., Sloan L., Thomas E. and Billups K. (2001) Trends, rhythms, and aberrations in global climate 65 Ma to present. *Science* **292**, 686–693.

Zachos J. C., Röhl U., Schellenberg A., Sluijs A., Hodell D. A., Kelly D. C., Thomas E., Nicolo M., Raffi I., Lourens L. J., McCarren H. and Kroon D. (2005) Rapid acidification of the ocean during the Paleocene-Eocene Thermal Maximum. *Science* **308**, 1611–1615.

Zeebe R. E. (2005) Stable boron isotope fractionation between dissolved $B(OH)_3$ and $B(OH)_4^-$. *Geochim. Cosmochim. Acta* **69**, 2753–2766.

Zeebe R. E. (2013) Time-dependent climate sensitivity and the legacy of anthropogenic greenhouse gas emissions. *Proc. Natl. Acad. Sci.* **110**, 13739–13744.

Zeebe R. E. and Sanyal A. (2002) Comparison of two potential strategies of planktonic foraminifera for house building: Mg^{2+} or H^+ removal? *Geochim. Cosmochim. Acta* **66**, 1159–1169.

Zeebe R. E. and Wolf-Gladrow D. A. (2001) *CO_2 in Seawater: equilibrium, Kinetics, Isotopes*. Elsevier Oceanography Series, Elsevier, Amsterdam.

Zeebe R. E., Sanyal A., Ortiz J. D. and Wolf-Gladrow D. A. (2001) A theoretical study of the kinetics of the boric acid-borate equilibrium in seawater. *Mar. Chem.* **73**, 113–124.

Zeebe R. E., Wolf-Gladrow D. A., Bijma J. and Hönisch B. (2003) Vital effects in foraminifera do not compromise the use of δ11B as a paleo-pH indicator: evidence from modeling. *Paleoceanography* **18**, 1043. http://dx.doi.org/10.1029/2003PA000881.

Zeebe R. E., Zachos J. C. and Dickens G. R. (2009) Carbon dioxide forcing alone insufficient to explain Palaeocene-Eocene Thermal Maximum warming. *Nat. Geosci.* **2**, 576–580.

Associate editor: Robert H. Byrne